

Eidgenössisches Departement für

Umwelt, Verkehr, Energie und Kommunikation UVEK

Bundesamt für Energie BFE

Energieforschung und Cleantech

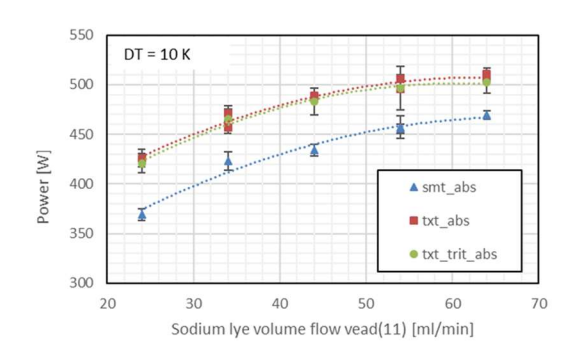
Final report dated 12.12.2019

## **ABSTOREX - Absorption Storage Experiment**

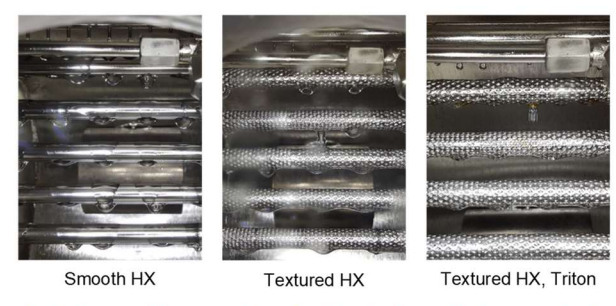
# Absorptionsspeicher - Experiment



ABSTOREX 1 kW liquid sorption facility



Power output for the heat exchanger's smooth (smt), textured tubes (txt), also with Triton surfactant addition



A higher surface wetting for the textured tubes and when using the Triton surfactant compared to smooth tubes

Source: © SPF 2019





Date: 12.12.2019

Location: Rapperswil

### Subsidiser:

Swiss Federal Office of Energy SFOE Energy Research and Cleantech Section CH-3003 Bern www.bfe.admin.ch

### Subsidy recipients:

SPF Institute for Solar Technology, HSR University of Applied Sciences Oberseestr. 10, CH-8640 Rapperswil

www.spf.ch

### Authors:

Xavier Daguenet, xavier.daguenet @spf.ch Paul Gantenbein, paul.gantenbein @spf.ch Mihaela Dudita, mihaela.dudita @spf.ch Lukas Omlin, lukas.omlin @spf.ch

With contributions from: Albert Trudel, Franz Steiner, Jérémy Corpataux, Jonas Müller, David Brönnimann, Jérémy Guillot, Daniel Lustenberger, Fabio Lichtensteiger, Loris Laib.

### SFOE project coordinators:

Andreas Eckmanns, andreas.eckmanns@bfe.admin.ch Elimar Frank, elimar.frank@frank-energy.com

SFOE contract number: SI/501232-01

All contents and conclusions are the sole responsibility of the authors.



## Zusammenfassung

Im Rahmen des EU-finanzierten Projektes COMTES haben die vom SPF zusammen mit der EMPA durchgeführten Untersuchungen gezeigt, dass in der Phase der Absorption die experimentell gemessene Leistung wesentlich tiefer ist als die theoretisch berechneten Werte. Basierend auf dieser Erfahrung, sowie der weiteren Anwendung der Rohrbündel-Technologie zur Formung eines Fallfilms für den Stoff- und Wärmeübergang im Absorber-Desorber (A-D) und im Verdampfer-Kondensator (E-C), wurde daher zur Optimierung der Reaktionszone im ABSTOREX Projekt ein 1 kW Prototyp entwickelt und aufgebaut. Nebst wässriger Natronlauge können in dieser Anlage weitere, eine potentiell hohe verfügbare Energiedichte aufweisende, Stoffpaarungen wie LiBr-H<sub>2</sub>O und LiCl-H<sub>2</sub>O für die Untersuchungen eingesetzt werden. Zu den drei Stoffpaarungen wurden die thermo-physikalischen Eigenschaften in Form von Gleichungen aufbereitet sowie numerische Modelle entwickelt.

Der Stoff- und Wärmeübertrager in der Reaktionszone - der Leistungseinheit - des Speichersystems hängt von der Rohrbündel-Oberflächenbenetzung durch die konzentrierte Lauge - dem Sorbent -, der Verweilzeit der Lauge im Wasserdampf sowie der Turbulenz im Fallfilm ab. Das Benetzungsverhalten der Oberfläche wird stark bestimmt durch die Oberflächenenergie der Stahlrohre in Kombination mit den Stoffeigenschaften der wässrigen Natronlauge. Die hohe Oberflächenspannung der konzentrierten Natronlauge spielt dabei eine entscheidende Rolle.

Im Hinblick zum Aufbau der 1 kW Anlage wurden umfangreiche Vorversuche zur Oberflächen-Benetzung und Verweilzeit gemacht. Eine verbesserte Oberflächen-Benetzung mit konzentrierter Sorbent-Lösung wurde erreicht mit folgenden Veränderungen der Oberflächen (Chemie): Zugabe von Weichmachern in die Sorbent-Lösung, Wärmebehandlung der Wärmeübertrager-Rohre sowie Texturierung der Oberfläche. Die Verweilzeit der Lösung im Wasserdampf und die Wasserdampf-Lösungs-Grenzschicht sowie die Benetzung können mit porösen SiC-Schäumen verbessert werden. Stabilitätsversuche mit Natronlauge und SiC-Industrieschäumen zeigten, dass diese nicht stabil sind, weil sie einen hohen Sauerstoffanteil haben sowie Metalle wie Eisen (Fe) und Aluminium (Al) enthalten. In Kontakt mit Natronlage gasen die Schäume aus und werden spröde. Auf den Einbau in die A-D Einheit der 1 kW Prototype wurde daher verzichtet.

Diese Ergebnisse flossen in die Planung sowie den Zusammen- und Einbau der Stoff- und Wärmeaustauscher für die A-D Einheit und die E-C Einheit der 1 kW Laboranlage ein. Am gewählten Aufbau können die Rohrbündel im A-D und im E-C leicht ausgetauscht werden. Hiermit wird eine hohe Flexibilität erreicht und es können die verschiedensten Rohrbündeltypen mit unterschiedlichen Oberflächenstrukturen (oder mit stabilen Keramikschäumen ummantelte Rohre) eingesetzt werden. Weiter können die Fluideigenschaften, wie Reduktion der Oberflächenspannung, mit "Weichmachern" beeinflusst werden.

In der 1 kW Anlage können die Prozesse der Leistungseinheit eines realen thermo-chemischen Speichersystems gefahren werden, da sie zudem die Fluidkreise für Sorbent und Sorbat umfasst. Die dazu notwendigen Komponenten wie Dosierpumpen, Sensoren zur Temperatur-, Durchfluss, Dichteund Gewichtsmessung wurden ausgewählt, kalibriert und installiert. Die einzelnen Bauteile sowie die aufgebaute Anlage wurden umfangreichen Lecktests unterzogen. Die erste Inbetriebnahme und die Funktion aller Bauteile im Verbund wurde mit destilliertem Wasser - sowohl auf der A-D als auch auf E-C durchgeführt. Messungen zeigten, mit Wasser der Seite Die dass eine Wärmeübertragungsleistung von 1 kW – zwischen A-D und E-C – erreicht wird.

Die Effizienz von zwei unterschiedlichen A-D Wärmetauschern – glatte und strukturierte Rohre - wurde mit dem Sorbent NaOH- $H_2O$  bestimmt. In den Desorptionsversuchen – Speicherbeladung – sind die Zielwerte mit 1.2 kW und einem Konzentrationsunterschied von 20 wt.% erreicht worden (Leistung Erhöhung von 20 % in Vergleich zur der Referenz Wärmetauscher mit glatten Rohre). Die besten



Resultate in der Absorption - Speicherentladung – wurden mit texturierten Rohren und einer Leistung von 0.72 kW und der Konzentrationsunterschied von 7.5 wt.% erzielt. Mit diesem nicht optimalen Konzentrationsunterschied liegt die theoretische Energiedichte mit rund 175 kWh/m³ doppel so hoch wie diese von einem sensiblen Wasserspeischer. Wobei der Einsatz von Triton QS-15 keine messbare Erhöhung der Leistung ergab, obwohl sich die Oberflächenbenetzung mit konzentrierter Lauge verbesserte.

Die aus den Messresultaten (ohne Triton) - bestimmten Stoff- ( $\beta$ ) und Wärmeübergangszahlen ( $\alpha$ ) erreichen Werte von  $\beta$  = 1 bis 6 g/(m²\*s) und  $\alpha$  = 250-400 W/(m²\*K) bei T(HTF in den A-D Rohren) = 35 °C und  $\alpha$  = 650-1000 W/(m²\*K) bei T(HTF in den A-D Rohren) = 25 °C. Vergleiche mit Literaturwerten für LiBr-H<sub>2</sub>O zeigen eine gute Übereinstimmung mit den  $\alpha$ -Werten, hingegen sind die gemessenen  $\beta$ -Werte tiefer als die Literaturwerte.

Die Optimierung des ABSTOREX Systems umfasst die Entwicklung, den Einbau und den Test eines Wärme- und Stoffübertragers mit einer grösseren Grenzfläche zwischen Natronlauge und Wasserdampf. Die Umsetzung des Konzepts mit Metallgeweben oder Schäumen um die Rohre würde die Verweilzeit der Lauge im Sorbat-Dampf erhöhen und damit zu einer besseren System-Effizienz führen (bei gleicher Baugrösse eine höhere Absorptionsleistung und eine grössere Konzentrationsdifferenz gekoppelt mit einer erhöhten Speicher-Energiedichte).

Eine Skalierung der Leistungseinheit zu einem Speichersystem für ein Einfamilienhaus oder ein Mehrfamilienhaus kann auf der Basis des numerischen Modells für die Sorbent-Sorbat-Paarung NaOH-H<sub>2</sub>O und Wasserdampf, gemacht werden.

Der Einsatz eines kompakten, saisonalen (Ab-) Sorptionsspeichers, dessen Konzept im ABSTOREX getestet wurde, kann den Wärmebedarf im Winter mit Solarenergie aus dem Sommer befriedigen.

## Résumé

Les recherches menées conjointement par le SPF et l'EMPA dans le cadre du projet européen COMTES ont montré que la puissance expérimentalement mesurée au cours du processus d'absorbtion est considérément plus faible que les prédictions théoriques. Dans le but d'optimiser la zone de réaction, un prototype de 1 kW basé sur la technologie de faisceau de tubes à film de sorbant ruisselant pour les échangeurs de chaleur combinés Absorbeur-Désorbeur (A-D) et Evaporateur-Condenser (E-C) a été conçu et construit. D'autres couples de matériaux présentant une densité énergétique potentiellement haute tels que LiBr-H<sub>2</sub>O et LiCl-H<sub>2</sub>O peuvent être caractérisés sur cette installation en plus de la soude caustique (NaOH-H<sub>2</sub>O). Les propriétés thermophysiques de ces couples de matériaux ont été collectées sous forme d'équations et des modèles numériques ont été développés.

Le mouillage des tubes constituant l'échangeur de chaleur et de matière, le temps de séjour du sorbant dans la vapeur ainsi que la turbulence dans le film ruisselant déterminent la puissance échangée au niveau de la zone de réaction (qui constitue l'unité de puissance du système de stockage). L'énergie de surface des tubes métalliques ainsi que les propriétés du sorbant déterminent fortement le mouillage de la surface de l'échangeur. Dans le cas de la soude caustique, la tension de surface élevée de ce sorbant joue un rôle déterminant.

De multiples expériences préliminaires de mouillage et d'optimisation de temps de séjour ont été effectuées pour préparer les mesures sur le prototype de 1 kW. Un meilleur mouillage de l'échangeur par la soude caustique concentrée a été obtenu par les solutions suivantes: addition de tensioactifs dans le sorbant, traitement thermique ou texturation de la surface des tubes constituant l'échangeur. Par ailleurs, l'utilisation de mousse céramique poreuse de type SiC permet d'augmenter le temps de



séjour de la solution, la surface de contact liquide/vapeur ainsi que la mouillabilité. Cependant, les tests de vieillissement de la mousse céramique SiC en contact avec de la soude caustique ne se sont pas avérés positifs certainement en raison d'une proportion d'oxygène élevée et de la présence de métaux tels que le fer (Fe) et l'aluminium (Al) contenus dans la mousse industrielle. Un dégazage a été constaté et la stabilité mécanique de la mousse se réduit au fil du temps; de fait il a été décidé de renoncer à l'utilisation de ce type de mousse dans l'unité A-D du prototype de 1 kW.

Ces résultats ont été pris en compte dans la conception tout comme dans le montage et l'assemblage des échangeurs de chaleur pour l'unité A-D et l'unité E-C du prototype de 1kW. Pour le montage expérimental choisi, les faisceaux de tubes sont facilement interchangeables. Cela permet une haute flexibilité et différent types de tubes avec différentes texturations (ou comportant un chemisage avec une mousse de céramique stable) peuvent être caractérisés. De plus, il est possible d'agir sur les propriétés des fluides (comme par exemple la réduction de la tension de surface en utilisant des tensioactifs).

Le prototype de 1 kW, comporte des circuits hydrauliques pour le sorbant ainsi que le sorbat, ce qui permet de conduire des expériences avec les mêmes conditions dans la zone de réaction que dans un stockage thermochimique réel. Les composants nécessaires au bon fonctionnement de l'installation comme les pompes pour le transfert des fluides (dont une pompe de dosage du côté du sorbant) tout comme les capteurs de mesure de température, débit, densité et de masse ont été choisis, calibrés et installés. Qui plus est, chaque composant tout comme l'installation finie a subi des tests d'étanchéité. Pour la mise en service, de l'eau a été utilisée pour les deux circuits (A-D tout comme E-C). Au cours de ces mesures, une puissance de 1 kW a pu être transférée entre l'A-D et l'E-C.

La caractérisation de deux échangeurs A-D différents (l'un comportant des tubes lisses, l'autre des tubes texturés) avec le sorbant NaOH-H<sub>2</sub>O a été effectué. Au cours des expériences de désorption (charge du stockage), les valeurs cibles ont été atteintes (puissance de 1.2 kW et différence de concentration de 20 wt.%). Au cours de mesures d'absorption (décharge du stockage), une puissance de 0.72 kW ainsi qu'une différence de concentration de 7.5 wt.% ont été atteints avec des tubes texturés (par rapport à l'échangeur de référence avec des tubes lisses, augmentation de la puissance de 20 %). Considérant cette différence de concentration (non optimale), la densité énergétique théorique est, avec environ 175 kWh/m³ supérieure au double de celle d'un stockage conventionnel à eau. L'utilisation d'un agent de mouillage (Triton QS-15) n'a pas engendré d'amélioration de ces valeurs en dépit d'un meilleur mouillage avec la soude caustique concentrée.

A partir des résultats de mesure (sans triton), les coéfficients de transfert de matière ( $\beta$ ) et de transfert de chaleur ( $\alpha$ ) ont été calculés et atteignent des valeurs  $\beta$  = 1 à 6 g/(m²\*s) et  $\alpha$  = 250 à 400 W/(m²\*K) pour T(HTF à l'entrée de l'AD) = 35 °C et  $\alpha$  = 650-1000 W/(m²\*K) pour T(HTF à l'entrée de l'AD) = 25 °C. Une comparaison avec des valeurs de la litérature pour le couple LiBr-H<sub>2</sub>O montrent une bonne adéquation en ce qui concerne les valeurs de transfert de chaleur. Les valeurs de transfert de matière sont par contre inférieures à celles de la littérature.

L'optimisation future du système ABSTOREX prévoit le développement, l'implémentation et le test d'un échangeur de chaleur et de matière offrant une grande surface de contact liquide/gaz. En effet, un concept d'échangeur basé sur un treillis ou une mousse placé autour des tubes devrait permettre d'augmenter le temps de séjour de la soude dans la vapeur d'eau ainsi que les performances du système (puissance plus élevée pour une même taille de réacteur, augmentation de la différence de concentration ainsi que de la densité énergétique associée du stockage).

Un dimensionnement de l'unité de puissance adaptée à un stockage pour une maison individuelle ou un immeuble d'habitations peut être mené à bien grâce au model numérique déveleppé pour le couple sorbant/sorbat NaOH-H<sub>2</sub>O. La mise en oeuvre d'un stockage saisonal compact basé sur le concept



testé au cours du projet ABSTOREX constitue une solution à long terme pour l'exploitation maximale du potentiel solaire en été en vue de couvrir les besoins en énergie thermique durant l'hiver.

## **Summary**

Investigations performed by SPF and EMPA researchers in the EU financed project COMTES have shown that during the absorption phase, a lower power compared to the theoretical value was obtained. Thus, following the tube bundle falling sorbent film technology and using a combined Absorber-Desorber (A-D) and Evaporator-Condenser (E-C) concept, a 1 kW prototype was developed in this consecutive Swiss national R&D project called ABSTOREX to optimize the heat and mass exchanger units. Beside aqueous sodium hydroxide (NaOH, lye), other sorbent pairs with high energy density like LiBr-H<sub>2</sub>O and LiCl-H<sub>2</sub>O were considered and numerical models were developed.

The heat and mass exchange in the reaction zone – the power unit – of the system depends on the sorbent wetting over the tube bundle surface of the heat and mass exchangers, on the sorbent residence time in the water vapour (sorbate) and on the flow turbulence in the falling film. The wetting behaviour strongly depends on the wetted surface characteristics of the metallic tubes and on sorbent thermophysical properties, especially the high surface tension at high NaOH concentration.

Extensive small-scale experiments related to surface wetting and residence time were performed. An improved surface wetting of the concentrated sorbent solutions was achieved by: addition of surfactants in the sorbent solution, thermal annealing of the tube bundle tubes and surface roughness optimisation (mechanical texturing). The liquid sorbent residence time as well as the gas-liquid interface in the water vapour was increased by the use of porous SiC foams. The tested ceramic foams have a good wetting behaviour with concentrated NaOH (50 wt.%). Aging experiments for the ceramic foams and concentrated sodium hydroxide solutions were made. The ceramic foams (SiC) are containing a high amount of oxygen, iron (Fe) and aluminium (Al), thus they were not stable for prolonged contact with sodium lye. For this reason, they were not implemented in the A-D unit of the 1 kW prototype.

The improvements from the small scale experiments were considered in the planning, assembling and implementation of the combined Absorption-Desorption (A-D) unit and in the Evaporation-Condensation (E-C) unit of a 1 kW laboratory test rig. A modular design was chosen for having the flexibility to replace the A-D and the E-C tube bundles of the units. This configuration allows testing of several types of tubes (outer surface roughness / wrapped with stable ceramic foam) and liquid sorbent modifications, e.g. by surfactant addition.

The 1 KW setup is able to emulate the working condition of the power unit of a real thermochemical heat storage and includes the full sorbent and sorbate loops. All the necessary components, e.g. dosing pumps, sensors for temperature, fluid flow, density and weight measurement were selected, calibrated and and tested considering the working environment (low pressure, vacuum tight and prolonged contact with alkaline solutions). Leakage tests were performed on separate components as well as on the assembled facility. Measurements with distilled water as working fluid on the A-D as well as on the E-C side were performed and a heat transfer power of 1 kW between the A-D and E-C units was reached.

The efficiency of two different A-D heat exchangers - with smooth and textured tubes - was determined with the sorbent NaOH-H<sub>2</sub>O. In the case of storage charging (desorption process), the target values were achieved: 1.2 kW power and 20 wt.% concentration difference resulted. The best results in the case of storage discharging (absorption process), were registered for the textured tubes (power increase of 20 % compared to the reference plain tubes heat exchanger). A power of 0.72 kW and a concentration



difference of 7.5 wt.% was obtained. With this non optimised concentration difference, a theoretical energy density of 175 kWh/m³ is reached, which is more than the double of a sensible water storage. The use of surfactants (e.g. Triton QS-15) has not considerable improved the power, however implementation of Triton in the A-D unit resulted in a better surface wetting of the concentrated lye over the tube bundles.

The mass ( $\beta$ ) and heat ( $\alpha$ ) transfer coefficient values (without the use of Triton surfactant) are  $\beta$  = 1 to 6 g/(m²\*s) and  $\alpha$  = 250-400 W/(m²\*K) at T(Heat Transfer Fluid - HTF in the A-D tubes)=35 °C und  $\alpha$  = 650-1000 W/(m²\*K) at T(HTF in the A-D tubes)=25 °C. A comparison to literature values of LiBr-H<sub>2</sub>O are showing similar  $\alpha$ -values. But the measured  $\beta$ -values are lower than reported in literature for LiBr-H<sub>2</sub>O.

Further optimization of the ABSTOREX system include the development, implementation and testing of a heat and mass exchanger with a larger contact area between the sodium lye and the water vapour. Concept like the use of mesh or foam around the tubes would result in longer residence times of the lye in the sorbate vapour as well as better performances of the system (higher absorption power with the same reactor size and higher concentration decrease, linked with an improved energy storage density.

A power unit upscaling to a higher power for single or a multi family house application can be done based on the numerical model developed for the sorbent pair: NaOH-H<sub>2</sub>O and water vapour. Implementation of a compact seasonal storage using the liquid sorption concept tested in ABSTOREX is a long-term solution for harvesting the maximum from the solar energy during summer and satisfying the need for thermal energy in wintertime.

## **Main findings**

- ABSTOREX project proposes a compact concept for seasonal energy storage of renewables based on liquid sorption technology, with the aim of a higher energy density than the state of water sensible water storage.
- A 1 kW testing facility fully equipped for researching different sorbent pairs and heat exchanger configuration as well as basic phenomena like evaporation or condensation at low pressure was successfully build and tested.
- The heat exchanger with optimized textured tubes evidenced an improved surface wetting, which lead to an absorption power increase of 20 % compared to plain tubes.
- Further improvement of the A-D unit (increasing of the liquid-gas surface and residence time) is suggested to be investigated.
- The numerical model developed for the NaOH-H<sub>2</sub>O and water vapour pair allows an upscaling to a higher power units for single or multifamily houses or industrial application. It will provide a long term and loss free storage solution for transferring the excess solar energy from summer and satisfying the need for thermal energy for space heating and domestic hot water during winter.



## **Contents**

1	Introduction	12
1.1	Background information and current situation	12
1.2	Numerical investigation on using different working pairs with a falling film heat a exchanger	
1.3	Purpose of the ABSTOREX project and concept description	14
1.4	Objectives	16
2	Improving the heat and mass transfer – preliminary surface wetting experiment	s 17
2.1	Theoretical methods for improving surface wetting	17
2.2	Experimental	18
2.3	Results and discussions	20
2.3.1	Reducing the surface tension of ABSTOREX sorbents	20
2.3.2	Initial surface wetting experiments	20
2.3.3	Experiments implementing different methods for improving the surface wetting	21
2.3.4	Investigations regarding the stability of surfactant and concentrated sodium hydroxide	
2.3.5	Increasing the residence time of the of the sorbent in the water vapour	24
3	One kilowatt laboratory test rig	28
3.1	Experimental setup	28
3.2	Heat and mass exchanger design and sizing	30
3.3	Facility building	33
3.4	Heat Transfer Fluid (HTF) loop	35
3.5	Control and DAQ	36
4	Facility Commissioning	38
4.1	Sensors selection and calibration	38
4.2	Leak test	40
4.3	Commissioning the facility	40
5	Process an method	43
5.1	Measurement and calculations	43
5.2	Raw measurements	43
5.3	Facility function tests	44
5.4	Measurement campaigns	45
6	Measurement results and discussion	47
6.1	Absorption measurements	47
611	Influence of the sorbent volume flow rate	47



6.1.2	Influence of the sorbent volume flow rate (textured tubes)	48
6.1.3	Influence of the temperature difference between Absorber and Evaporator inlet for textured heat exchanger	
6.1.4	Impact of the use of surfactant	51
6.2	Desorption measurements	52
6.3	Post processing results	53
6.4	System assessment	56
7	Conclusions	57
8	Outlook	58
9	National and international collaboration	58
10	Communication	59
11	Publications	59
12	References	61
13	Annex	64
Annex	1: Laboratory test rig sensor nomenclature	64
Annex	2: Laboratory test rig active elements and components nomenclature	65
Annex	3: Overview of conducted experiments and comparison with COMTES project	66



## **Abbreviations**

A-D Absorber-Desorber

DAQ Data acquisition

E-C **Evaporator-Condenser** 

**GUI** Graphical User Interface

HAM Heat and Mass transfer

НΧ Heat exchanger

**HTF** Heat Transfer Fluid

LHS Latent Heat Storage NI **National Instruments** 

of reading or

**PCM** Phase Change Material

**PBS** Phosphate Buffered Saline

SHS Sensible Heat Storage

**TES** Thermal Energy Storage

THS Thermochemical Heat Storage

### **Symbols**

 $\mathsf{GTL}_\mathsf{D}$ (K) Gross temperature lifts for desorption

**GTLs** Gross temperature lifts for sorption (K)

Н (kJ/mol) Molar enthalpy

h (kJ/kg) Specific enthalpy

(A) Electrical current

(%) Uncertainty In

(mm) Level Lv

Molecular weight Μ (g)

m (kg) Mass

(kg/s) Mass flow rate ṁ

(mol) Mole number of a substance n

(mbar) Pressure

Q (kJ) Thermal energy  $Q_d$ 

 $(kWh/m^3)$ **Energy density** 



(mbar·l/s) Leakage rate q (°C) Т Temperature t (s) Time ΤE (-) Temperature effectiveness ٧ Volume (l) Ÿ (ml/min) Volume flow rate

x(T,P) (kg<sub>sorbate</sub>/kg<sub>sorbent</sub>) (weight %) Load / sorbate uptake

### Greek symbols



### 1 Introduction

### 1.1 Background information and current situation

Deployment of clean energy technologies is addressing the global challenges like energy security, climate change and sustainable development. Solar thermal energy is a low-carbon alternative to conventional fuels. It has still an untapped potential for covering the buildings heat demand, which represents 47% from the global energy demand, according to the International Energy Agency. One of the main challenge by using solar thermal energy for space heating is the temporal dephasing between the solar energy availability and the heating demand. Moreover, due to the low heat demand in summer, a significant amount of heat is wasted. Thermal Energy Storage (TES) is a solution for harvesting the maximum from the solar energy during summer and it can significantly contribute to the need for thermal energy in wintertime. Moreover, TES can be used in combination with other heat sources, for example geothermal energy or industrial waste heat. TES systems have environmental and economic benefits, particularly when harvesting the freely available energy from a renewable source.

Different materials can be used to store thermal energy (Akeiber et al., 2016; Xu et al., 2014). The criteria for material's selection is related to the thermo-physical properties. The aimed material characteristics are suitable melting point, high latent heat, high specific heat, and high thermal conductivity. Chemical and thermal stability, low volume change, low vapour pressure, low supercooling, compatibility with metal containers, easy availability, non-toxic and cost are also relevant. Depending on the type of material selected for heat or cold storage, TES systems can be classified into three categories (Alva et al., 2018):

- sensible heat storage, e.g. using water when the amount of stored heat is directly influenced by the material's mass, thus density, specific heat and temperature variation.
- latent heat: materials store heat in their latent heat during a constant temperature process,
   e.g. Phase Change Materials (PCM); the latent heat is 50-100 times larger than sensible heat
   and the energy storage density near the phase change temperature is very high, thus
   recommending the PCMs for compact TES systems;
- chemical heat storage: uses reversible reactions where the heat absorbed or released depends on the reaction enthalpy, calculated based on the standard enthalpy of formation.

Sensible heat storage systems are state of art, there is an extensive research running for improving the latent heat storage materials and chemical heat storage. Comprehensive research and review papers on thermal energy storage systems are available (Alva et al., 2018; Alzoubi et al., 2017; Arteconi et al., 2013; Daguenet-Frick et al., 2017a; Delgado et al., 2012). Closed-sorption heat storage based on water vapour absorption in sodium hydroxide solution can achieve a significantly higher volumetric energy density compared to sensible hot water storage (Daguenet-Frick et al., 2015).

ABSTOREX project is a follow-up of the European COMTES project, in which researchers from SPF and EMPA developed a compact thermal storage technology based on liquid sorption concept. Their investigations have shown that during storage discharging (absorption phase), a lower power compared to the theoretical value was obtained. This behaviour was explained by the poor wetting of the sorbent (concentrated sodium hydroxide - NaOH lye) over the heat exchanger's (HX) tube surface, a low residence time of the lye in the water vapour phase and low a flow turbulence in the sorbent. Thus, a



1 kW prototype was developed in this consecutive Swiss national R&D project to implement different solutions for overcoming these drawbacks and to further optimize the heat and mass exchanger units.

The report contains five main sections describing the experimental facility, the small scale wetting experiments and the implementation of surface wetting concepts into the 1kW laboratory test. Moreover, absorption and desorption measurements and influence of different operation parameters is discussed.

The description of existing storage technologies and a short introduction into the ABSTOREX concept in made Section 1. Compared to sensible and latent technologies, closed-sorption heat storage can achieve a significantly higher volumetric energy density compared to sensible hot water storage.

The description of the 1 kW laboratory test rig is made in Section 3, while the facility commissioning is shown in Section 4. A precise temperature characterization of the Heat and Mass Exchangers and of the Heat Transfer Fluid (HTF) loops is done by the use of 40 calibrated temperature sensors. The flow rate is determined for each HTF, sorbent and sorbate loop by the use of 2 magnetic inductive sensors, 1 Coriolis sensor and 1 oval-wheel-sensor. Measurements with distilled water as working fluid in the A-D and in the E-C side were performed and a heat transfer power of 1 kW between the A-D and E-C units was reached. All components like dosing pumps, sensors for temperature, fluid flow, density and weight measurement were selected, calibrated and tested considering the working environment (low pressure, vacuum tight and prolonged contact with alkaline solutions). Leakage tests were performed on separate components as well as on the assembled facility.

The dedicated applications are described in Section 5 and they were made in LabVIEW (data acquisition), in Matlab (data handling) and in Excel (for comparing the results and the effect of different parameters). The control and data acquisition software is based on NI LabVIEW (JKI) state machine templates. The operation of the software can be done in "manual control" or "automatic control" mode. The measurements results and the effect of different parameters is shown in Section 6.

# 1.2 Numerical investigation on using different working pairs with a falling film heat and mass exchanger

A preliminary assessment of different sorbet pairs was made. The properties of three sorbent pairs were implemented in the numerical model developed in the frame of the EU project COMTES (Daguenet-Frick et al., 2015). This model enables a sizing of the heat and mass exchangers (Desorber, Condenser, Absorber and Evaporator) constituting the reaction zone.

The physical and thermal properties for different sorbent materials are given by several authors (Conde, 2004; Florides et al., 2003; Lee et al.; Löwer, 1960, 1961; Pátek and Klomfar, 2006; Patterson and Perez-Blanco, 1988). The results of the modelling (based on the sorbent properties) are used to assess the potential of LiCl and LiBr and to compare them with the sorption heat storage based on NaOH.

As system boundary conditions, the upper concentration is limited to 50 wt.% for sodium hydroxide due to crystallization hazards at higher concentration and room temperatures. The upper concentration limitations for LiBr and LiCl are about 55 wt.% and 40 wt.% respectively. The bottom concentrations are defined by the minimal exploitable temperature by the single family passive house (about 32 to 35 °C are considered to be required at the inlet of a modern ground heating system). For these temperature level, a concentration of 30 wt.% for NaOH and LiCl, repsectively 40 wt.% for LiBr is required.

The heat and mass exchanger geometry considered is 4\*18 tubes tube bundle with a length of 300 mm for the combined Absorber-Desorber unit and a 16\*12 tubes tube bundle with a length of 700 mm for the Evaporator-Condenser unit.



According to this first numerical investigation, other sorbent-sorbate pairs like LiBr-H<sub>2</sub>O and LiCl-H<sub>2</sub>O could be used without major geometry modifications on the tube bundle heat and mass exchangers developed in the frame of the EU financed COMTES project.

However, the additional cost caused by the chemicals higher market price as well as energy density issues have to be considered.

### 1.3 Purpose of the ABSTOREX project and concept description

The focus in the ABSTOREX project is on the optimization of a heat and mass transfer unit with low power consumption that can be used for seasonal energy storage using a liquid sorption concept. Different sorbent pairs with high energy density are investigated: NaOH-H<sub>2</sub>O, LiBr-H<sub>2</sub>O and LiCl-H<sub>2</sub>O. The thermo-physical properties obtained from literature were processed, models were developed and mass and heat transfer characteristics were determined for the thermal fluid NaOH-H<sub>2</sub>O. These data are required for upscaling the ABSTOREX system to higher power.

In case of water vapour absorption in the liquid sorbent NaOH-H<sub>2</sub>O (Olsson et al., 1997), LiCl-H<sub>2</sub>O (Conde, 2004), LiBr-H<sub>2</sub>O (Loewer, 1960), the heat of evaporation  $\Delta h_v$  (2013) plus the absorption potential  $\Delta F$  are released (Aristov, 2014; Dubinin, 1960). As a result, the final temperature of the diluted solution is higher than the initial one. Regarding the heat storage potential of the sorbent-sorbate combinations, this method - the calculation of  $\Delta F$  - allows a comparison (Figure 1). Due to economic reasons, sodium lye was the first choice in this project, with the option of using the other two sorbent-sorbate combinations (LiBr-H<sub>2</sub>O and LiCl-H<sub>2</sub>O)<sup>1</sup>.

$$NaOH \cdot mH_2O + nH_2O \Leftrightarrow NaOH \cdot (m+n)H_2O + heat$$
 Eq. 1

The ABSTOREX thermochemical storage concept is based on water absorption/desorption in aqueous sodium hydroxide (NaOH) solution. The process shown in Eq. 1 achieves theoretically a significantly higher volumetric energy density compared to sensible water storage (Daguenet-Frick et al., 2015).

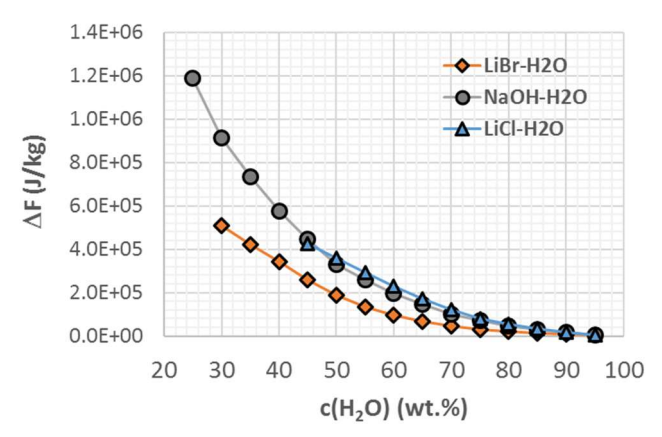


Figure 1: Absorption potential  $\Delta F$  in function of concentration  $c(H_2O)$  in the solution. The calculation is performed according the Polanyi-Dubinin, Clausius-Clapeyron and van t'Hoff theories. In the concentration range (H<sub>2</sub>O; 45 wt.% to 100 wt.%) NaOH-H<sub>2</sub>O and LiCl-H<sub>2</sub>O have the same potential. Doe to crystallisation (pumping the solution) and process pressure reasons, both solutions are restricted to a) NaOH-H<sub>2</sub>O 50 wt.% to 75 wt.% and b) LiCl-H<sub>2</sub>O 55 wt.% to 75 wt.%.

The main components and also the charging and the discharging processes are represented schematically in Figure 2 and Figure 3. The reaction zone consists of two main units: A-D (Absorber-Desorber) and E-C (Evaporator-Condenser). The system was designed to allow the separation of

14/66

<sup>&</sup>lt;sup>1</sup> The laboratory design allows the process for liquid sorbent-sorbate combinations.



capacity (which is given by the volume of the storage tanks for the sorbent - NaOH-H<sub>2</sub>O and sorbate - H<sub>2</sub>O) and power (given by the heat and mass exchangers' active area). As the absorption and evaporation process steps take place in winter, while the desorption and condensation process steps in summer, the Absorber and Desorber was combined in one unit as well as the Evaporator and Condenser in a second unit. This reduces considerably the volume used for the storage system.

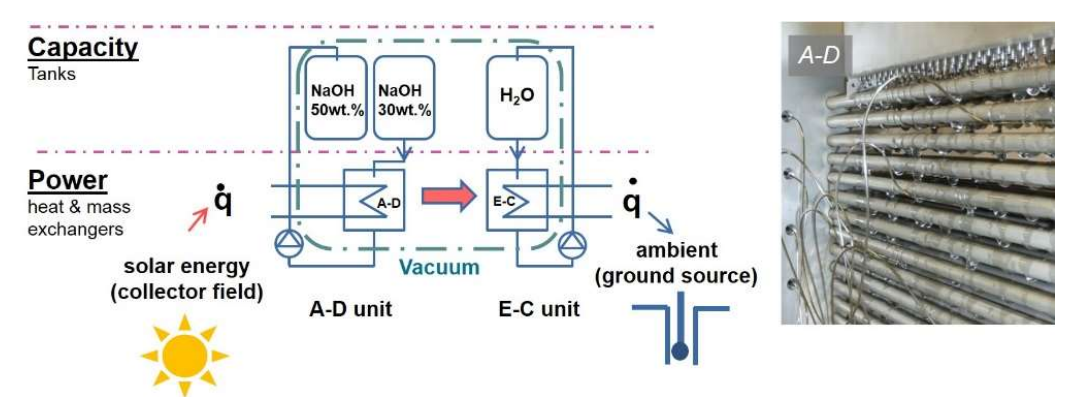


Figure 2: Charging process in summer time (desorption process).

The charging process occurs in summer using the heat from a renewable source to partially evaporate the water from the liquid sorbent, a diluted sodium hydroxide solution (30 wt.%). By using solar thermal collectors and heat at low temperature from the environment, a high renewable energy fraction can be obtained. The charging process takes place in the Desorber unit, which consists of a falling film tube bundle heat and mass exchanger. This chamber is used for the desorption process, as well as for the absorption (discharging in winter). Combination of two process steps in one single chamber is possible because of seasonally shifted charging and discharging processes. The concentrated sodium lye solution (50 wt.%) and the water is stored without significant thermal losses until the discharging process occurs. The latent condensation heat from the water vapour is released to a ground sink (e.g. a borehole), while the condensed water is stored in a separate tank at room temperature.

A reversed process takes places during discharging. A low temperature thermal input (a ground source) is used for water evaporation under reduced pressure in the Evaporator unit. By combining the concentrated sorbent with water vapour in the Absorber unit, the stored chemical energy is recovered as heat. The ABSTOREX system can be used both for space heating and domestic hot water.

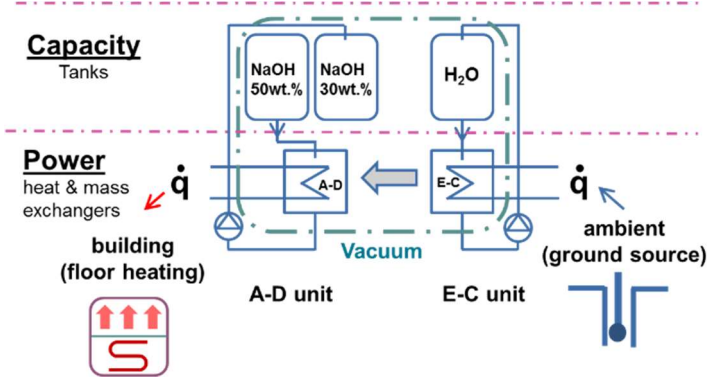
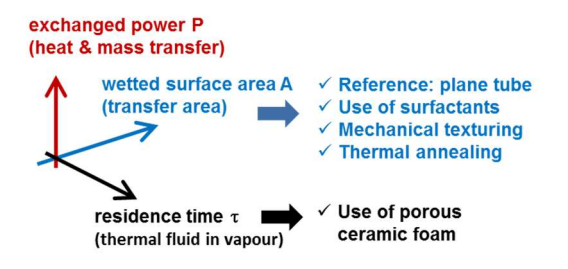


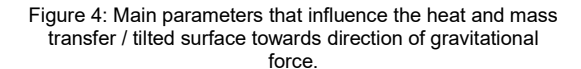
Figure 3: Discharging process in winter time (absorption process).



The main parameters influencing the heat and mass transfer are shown in Figure 4. The tube bundle falling film heat and mass transfer concept is adopted in the ABSTOREX project due to the simple design, low costs, and high heat transfer rates.

Previous experiments made in the EU COMTES project have indicated a low temperature lift at low design mass flow rates (aimed for a low pump energy consumption) during discharging (absorption phase). This behaviour was explained by the poor wetting (Figure 5) of the concentrated NaOH solution (50 wt.%) over the tube surfaces (AISI 316L), a low residence time of the lye in the water vapour phase and low turbulence in the sorbent (diffusion controlled mass transfer). The concentration is limited to 50 wt.% due to crystallisation reasons of concentrated sodium lye at room temperature <sup>2</sup>.





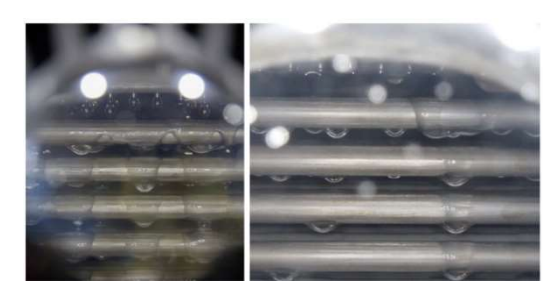


Figure 5: Poor wetting of NaOH – H<sub>2</sub>O (50 wt.%) over the tube bundle surface (flow rate 0.4 L/min) with visible dry spots, thus a smaller area for the heat and mass transfer.

To overcome these drawbacks, small-scale experiments such as fluid wetting improvements when surfactants are used, tube surface modification, and use of ceramic foams were performed and the results are briefly presented in Section 2 of this report. Further, a 1 kW laboratory test rig was designed to implement and assess the main findings from the small scale experiments. The test rig was designed to be able to emulate the working condition of a power unit from a real thermochemical heat storage. The results from the 1 kW test rig are presented in Section 3 to 6.

### 1.4 Objectives

The technical and scientific objectives of the project are:

- To identify sorbent material pairs with high energy density in order to store thermal energy in an absorption process (2-components and 2-phases);
- To design and develop a 1 kW laboratory test facility in which absorption / desorption and evaporation / condensation cycles can be performed with controlled boundary conditions;
- To carry out experiments to determine the heat and mass transfer coefficients and to evaluate the results;
- To propose a technological transfer to COMTES plant and reporting.

<sup>&</sup>lt;sup>2</sup> With a concentration > 50 wt.% a higher energy density could be reached, but pumping would be difficult and the reaction zone design would be more complex.



# 2 Improving the heat and mass transfer – preliminary surface wetting experiments

### 2.1 Theoretical methods for improving surface wetting

Previous experiments made in the COMTES project have indicated a low temperature lift due to poor tube surface wetting with concentrated NaOH-H<sub>2</sub>O (50 wt.%). Moreover, a low residence time of the lye in the vapour phase was recorded.

The preliminary surface wetting experiments were made to improve the heat and mass transfer in the tube bundle. Wettability of a solid by a liquid can be evaluated by measuring the contact angle ( $\theta$ , Figure 6) determined at the intersection of the liquid-solid interface and the liquid-vapour interface. The contact angle is defined by the Young equation, considering the three interfacial tensions:  $\gamma_{IV}$ ,  $\gamma_{SV}$  and  $\gamma_{SI}$  - the liquid-vapour, solid-vapour, and solid-liquid interfacial tensions, respectively, and  $\theta_Y$  the contact angle.

Liquids with lower surface tension (Figure 7) will allow a better wetting of the surface. The wetting force is directly influenced by the liquid surface tension and it is defined (Eq. 2), where p is the perimeter of the contact line and  $\theta$  is the contact angle.

$$F = \gamma_{lv} \cdot p \cdot cos\theta$$
 Eq. 2

As the ABSTOREX sorbent is an aqueous solution, a hydrophilic surface is desired for improving the surface wetting (Figure 8).



Figure 6: Contact angle formed by sessile liquid drop on a smooth homogeneous solid surface (Yuan and Lee, 2013).

Figure 7: Unbalanced forces from the liquid molecules at the surface determines the surface tension (Yuan and Lee, 2013).

Figure 8: Surface wetting: A - partial wetting (hydrophilic surfaces, when the liquid is water, B - complete non-wetting (hydrophobic surface when the liquid is water), C - complete wetting.

Thus, surface wetting can be improved by modifying the liquid's properties like surface tension (lowering the surface tension) or by changing the solid surface structure and chemistry.

The surface tension is decreasing when temperature is increasing and sorbent concentration is decreasing. Therefore, the highest value of the surface tension is expected for the concentrated sorbent solution (e.g. for ABSTOREX: 50 wt.%) at room temperature. To assess the baseline situations, the initial wetting experiments were made using these conditions: room temperature, concentrated sodium hydroxide and plain stainless steel tubes similar with the ones from the COMTES tube bundle HEX.

Since liquids with lower surface tension values allow a better wetting of the surface, the influence of adding surfactants was investigated. Surfactants used in very low concentration (in the range of parts per million or milligrams per liter) can significantly decrease the surface tension of a liquid. The ability of the surfactant to reduce the surface tension is due to both hydrophilic and hydrophobic (chemical) components of the molecules (Tracton, 2006). Two surfactants were chosen for our study considering their stability in hot alkaline solutions: dihexyl sulfosuccinate sodium salt (DHSS) and Triton™ QS-15.



Dihexyl sulfosuccinate sodium salt is part of the sulfosuccinates class of anionic surfactants. DHSS has a low surface tension (30 mN/mm, ring method) and a high wetting power (a high potential to decrease surface tension). The wetting power is related to the wetting time (Jurado et al., 2010). Previous studies were performed on the wetting properties and stability of di-alkyl sulfosuccinate salts under extreme pH (until max 12) and temperature (max 80°C). It was shown that DHSS is stable in alkaline solutions at high temperature up to 80°C (Majmudar, 2014), which is at the desorption temperature level in a sodium hydroxide sorption heat storage.

Triton™ QS-15 is an anionic surfactant based on polyether sulfate (C12–14-tert-alkyl-ethoxylated sodium sulfate). It is soluble and stable in hot alkaline solutions, biodegradable and it will not persist in the environment. It is used for highly alkaline metal cleaners, bottle washing, zinc plating brightener, gas well cleaning, steam cleaners, etc.

The surfactant efficiency depends on the surfactant structure and concentration, on the solid surface properties (e.g. composition, pore structure, surface roughness), the pH value and temperature.

The second category of methods for wetting improving is related to solid surfaces modifications. Three mechanisms can be employed: mechanical, physical and chemical. Better wetting is promoted when a large surface area is in contact with the liquid. Higher surface area is obtained by varying the surface roughness and mechanical texturing. According to Wenzel's equation, increased roughness will decrease the contact angle on hydrophilic surfaces. Thus, roughness amplifies hydrophilicity, but not necessarily linearly (Brutin, 2015).

In order to modify the surface chemistry, more techniques can be applied, e.g. changing the surface functional groups (Trigwell and Selvaduray, 2006). Studies have shown that a heat treatment is increasing the chromium oxide (AISI 316L) content in the surface (Williams, 2011). This would promote a better wetting due to the formation of physical bonding with the polar groups from the aqueous sodium hydroxide solution. Moreover, it is favourable to have chromium and nickel oxide on the surface also due to corrosion issues i.e. improving the corrosion resistance.

Different surface treatments were reported to have different effects on the surface oxide content (Trigwell and Selvaduray, 2006). For example, the Cr (and thus Cr oxides) concentration decreases, while the Fe concentration increases in the case of mechanically polishing process. In addition, the surface nickel content is reduced to about 3%. After mechanically polishing, Cr is mainly bounded in the oxide form (Cr<sub>2</sub>O<sub>3</sub>). The oxygen bonding in the oxide form is reduced by electro-polishing, simultaneous to a considerably increase in oxygen bonding as hydroxide. This is because the process is done in an aqueous environment (containing OH-). An enrichment of chromium on the surface oxide layer normally occurs when stainless steel is electro-polished (Trigwell and Selvaduray, 2006).

Studies have shown that among all metal elements contained in the surface of AISI 316L, the Cr, Ni and Mo content can be modified due to heat treatment. Chromium and nickel – in theirs oxides forms- are the corrosion resistant elements. A heat treatment was reported to increase the chromium oxide content in the surface. The largest Cr and Ni ratio was obtained for 316L at a heating temperature of 300°C (Williams, 2011).

### 2.2 Experimental

The following chemicals were involved in the wetting experiments:

- sorbents to be used in the ABSTOREX heat and mass exchanger:



- sodium hydroxide (NaOH), 50 wt.% in H<sub>2</sub>O, density: 1.515 g/mL at 25 °C, surface tension: 116.72 mN/m; from this stock solution, a 45 wt.% solution with surfactant was prepared;
- o lithium bromide (LiBr), 54 wt. % in H2O, density: 1.57 g/mL at 25 °C, surface tension: 86.1 mN/m;

### wetting agent:

- di-hexyl sulfosuccinate sodium salt (DHSS) (technical, ~80 wt.% in H<sub>2</sub>O, Sigma Aldrich code 86146), CAS number 3006-15-3, chemical formula C16H29NaO7S, molecular weight: 388.45 g/mol;
- TRITON™ QS-15 (Trademark of The Dow Chemical Company, 100 wt.%, Sigma Aldrich code QS15), CAS Number 11105-10-5, chemical description: polyether sulfate, anionic surfactant;
- cleaning agent: acetone (technical, CAS number: 67-64-1, chemical formula: CH<sub>3</sub>COCH<sub>3</sub>, molecular weight: 58.08 g/mol) and ethanol (technical, CAS Number 64-17-5, chemical formula CH<sub>3</sub>CH<sub>2</sub>OH, molecular weight 46.07)
- deionized water (HSR, electrical conductivity between 2 to 15 μS/cm).
- The samples used are:
  - stainless steel tubes (1.4404), D<sub>ext</sub>=12 mm, with flat surface or different surface texturing;
  - a porous metallic sample supplied by the Fraunhofer-Institut für Fertigungstechnik und Angewandte Materialforschung IFAM (Dresden) made of stainless steel fibres (1.4841); the geometric dimensions of the sample are 30.05 mm x 30.15 mm x 2.1 mm, and the porosity is 61 vol.%.
  - porous SiC ceramic foams Hofmann CERAMIC GmbH with porosity ranging from 10 to 30 PPI (pores per inch).

Prior to the surface wetting experiments, the samples were first washed with demineralized water and then with ethanol or acetone. The porous samples were dried either with gaseous N2 (the metallic sample) or in an air furnace for min. 1 h (the SiC samples).

To avoid carbonization of the sodium hydroxide with  $CO_2$  from the air, the wetting experiments were performed into a glove bag (ca. 94x94x64 cm) filled with 4.5  $N_2$  (purity  $\geq$ 99.995%). The  $N_2$  functions as the inert gas.

A computer-controlled multipurpose tensiometer (Sigma 700, Biolin Scientific) was used for high precision measurements of surface tension and study of the surfactant effect on reducing the surface tension. The software OneAttension Version 1.6 was used. The basic principle of the Sigma measurement is to record and analyse the forces exerted onto a probe or solid sample using a sensitive microbalance. The force exerted on the balance can be converted into surface tension when a specific probe (Wilhelmy plate, Du Noüy or other) is used for drawing up the liquid in a meniscus. The autocalibrating microbalance can measure over a wide range with high accuracy (0.01 mg), for a maximum load of 210 g.



### 2.3 Results and discussions

### 2.3.1 Reducing the surface tension of ABSTOREX sorbents

The effect of surfactants on reducing the surface tension of the concentrated sodium hydroxide solution was studied using a Sigma 700 tensiometer from Transilvania University of Brasov (Romania). Different surfactant solutions (0.1 wt.%, 0.3 wt.%, 0.5 wt.%) were prepared, starting from the stock concentrate solution (1 wt.%) of DHSS (initial concentration 80 wt.%). Previous research studies recommend the use of DHSS in low concentration, e.g. from 0.1 to 0.5 wt.% (Majmudar, 2014). Our experimental studies indicated that the DHSS surfactant is reducing considerably the solution surface tension (Figure 9).

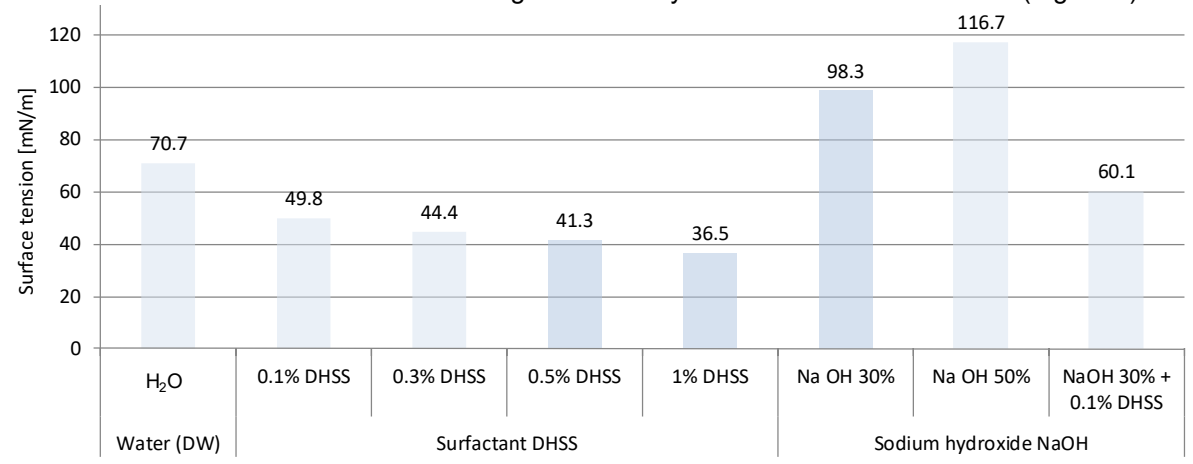


Figure 9: The influence of the DHSS surfactant on the surface tension values of concentrated sodium hydroxide solution.

### 2.3.2 Initial surface wetting experiments

Preliminary surface wetting experiments for two possible sorbent materials (NaOH-H<sub>2</sub>O and LiBr-H<sub>2</sub>O) on stainless steel substrates (plain/textured in one axial direction and one porous samples from Fraunhofer IFAM) were performed with or without the addition of DHSS surfactant. A poor wetting of the concentrated lye was recorded in both cases (Figure 10, left), where stable droplets were recorded.

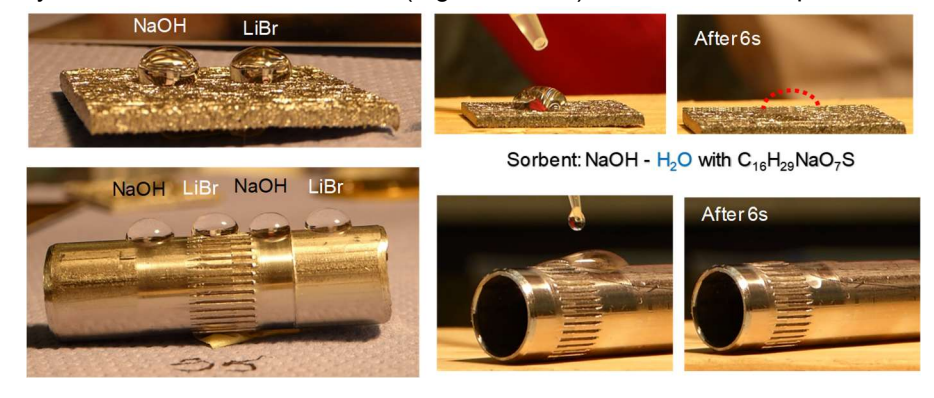


Figure 10: Surface wetting experiments with concentrated solutions of NaOH- $H_2O$  and LiBr- $H_2O$ ) on stainless steel substrates (porous and plain/textured in one axial direction indicating an improved wetting behaviour after the addition of DHSS surfactant ( $C_{16}H_{29}NaO_7S$ ).

The poor surface wetting behaviour is explained by the high surface tension of the concentrated sodium hydroxide solution (116.72 mN/m for NaOH 50 wt.% at 20°C) and by the rather poor hydrophilic



behaviour of the fibres. Water has also a rather high surface tension of 72.86 mN/m at 20°C. An improved wetting was obtained for both cases when adding the DHSS surfactant (Figure 10, right).

### 2.3.3 Experiments implementing different methods for improving the surface wetting

Surface modifications by texturing or annealing and fluid properties tuning by using surfactants were experimentally investigated. The aim of these experiments was to test the influence of different surface texturing on the wetting with concentrated sodium hydroxide and lithium bromide, with/or without surfactant addition. The surfactant stability is another aspect which was investigated. Moreover, a heat treatment for the stainless steel tubes used in the heat and mass transfer unit was also performed to improve the wetting.

Different tubes with a flat surface or structured (with horizontal, perpendicular or cross grooves) made from stainless steel AISI 316L were used. The heat treatment in air at  $300^{\circ}$ C was applied for the optimum surface textured tube and for a plane tube. In order to avoid the influence of gravity, small volumes (100  $\mu$ L) were used for the wetting experiments. When the radius of the droplet is much smaller than the capillary length, the effects due to gravity are negligible.

The influence of the two selected surfactants (DHSS and Triton™ QS-15) added in concentrated NaOH solutions on the wetting of the as received plane tubes was investigated. A solution of NaOH 45 wt.% was considered as reference. The surfactants had the same concentration (1000 ppm). In order to quantify the wetting of the fluid over the tube, wetting time was used (Stache, 1995). This was defined as the shortest time until the drop (100 µL) wets and falls over the tube. Both surfactants lead to good wetting, compared to the only sodium lye case (Figure 11). In the reference case, the droplet was stable for minutes.

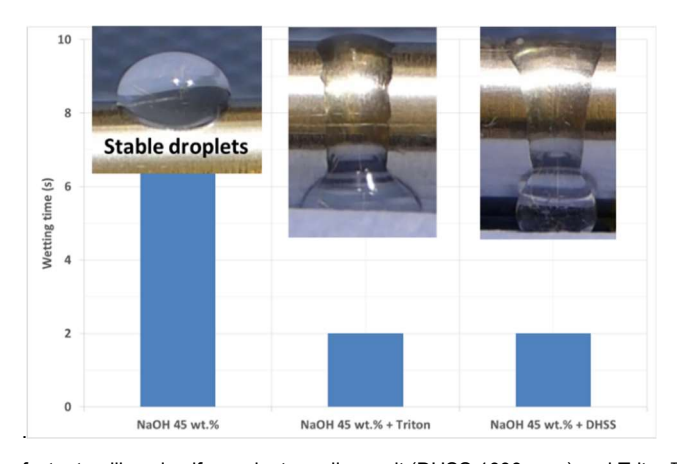


Figure 11: Influence of the surfactants: dihexyl sulfosuccinate sodium salt (DHSS 1000 ppm) and Triton™ QS-15 (1000 ppm) on the wetting time.

The influence of different surface texturing on the wetting with concentrated sodium hydroxide, without/or with surfactant addition (DHSS 100 ppm) was assessed. Compared to the reference case (S0), where the aqueous concentrated sodium hydroxide solution forms stable droplets, all the textured tubes present better wetting (Figure 12). The surfactant addition leads to a better wetting, decreasing the wetting time.

The best results were obtained in the case of sample S4. This pattern is also used in sodium heat pipes to improve the wetting (Bacanu, 1991). It was proven to have good durability in highly corrosive environments. Sample S1, with very small fines in the axial direction is a promising solution that can have good residence time. Sample S3 has lower wetting compared to the others due to the hill like



structures. In the case of S5 and S6, good wetting can be achieved, but the vertical fins limit the fluid spreading.

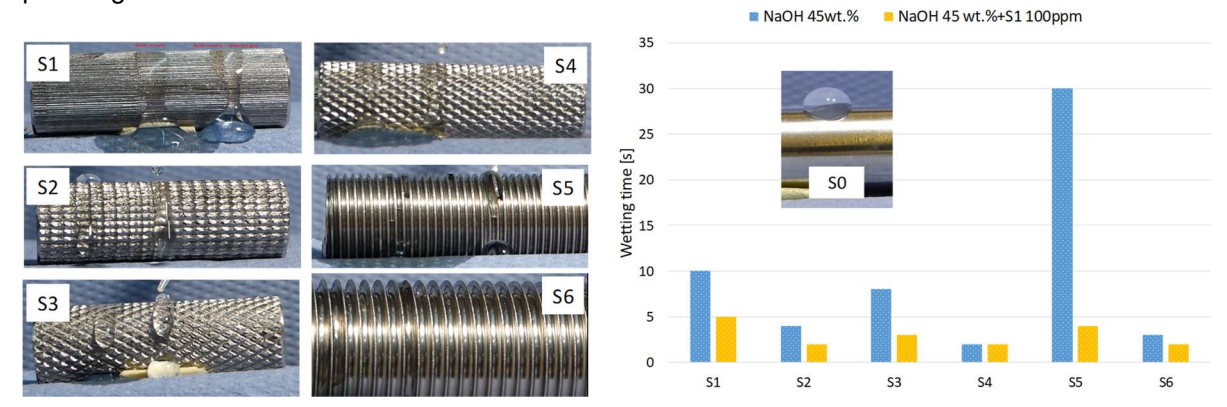


Figure 12: Influence of surface texturing and surfactant (dihexyl sulfosuccinate sodium salt, DHSS 100 ppm) on the surface wetting.

Annealing in air increases the surface metal oxide (Cr-oxide) content. A plane tube (as received) and the optimum textured tube (S4) were thermally treated for 1h, 2h and 3h at 300°C. Wetting experiments were performed by placing a 100µL droplet of concentrated sodium hydroxide solution (45 wt.%), without surfactant or with the addition of Triton™ QS-15 (T 1000 ppm). A better wetting was obtained for all the annealed samples (Figure 13). The good wetting time values can be explained by physical bonding formation between active groups from the testing fluid and from the metal surface. In the case of sample A1, very small droplets were added. This has led to a rather stable droplet, with higher wetting time.

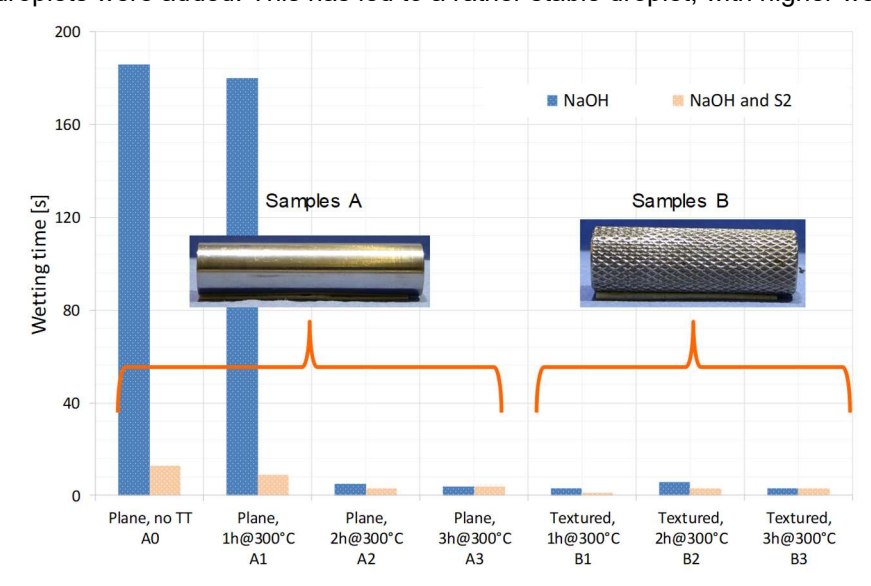


Figure 13: Influence of thermal treatment on the wetting time for two types of surfaces (plane and textured) and for sodium hydroxide with and without surfactant (S2, Triton™ QS-15 1000 ppm).

Moreover, in the heat and mass exchanger from the 1kW prototype, a manifold nozzle will be used. This was simulated by placing three large droplets (1000  $\mu$ l of testing fluid, see inset image from Figure 14) compared to the standard experiments where small droplets were used (100  $\mu$ L). The pipet diameter was similar with the nozzle diameter from the prototype system. A better spreading was observed in the case of the textured tube compared to the plane tube.

Another theoretical method proposed in Section 2.1 is the use of hydrophilic coatings. A feasibility study regarding the effect of hydrophilic coatings for improving the wetting of the tube bundle heat exchanger



was performed for different flat and textured tubes. The main goal was to improve the surface wetting by surface functionalization.

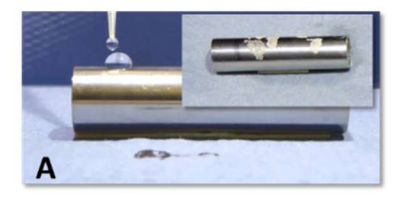


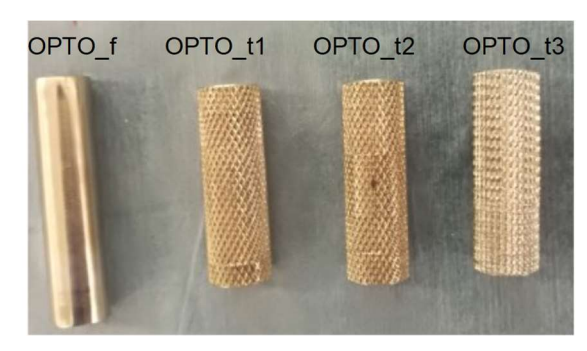




Figure 14: Comparison between wetting of sodium hydroxide 45 wt.% and different tube surfaces – plane tube as received (A), plane tube, thermally treated for 2 hours at 300°C (B) and optimized textured tube, thermally treated for 3 hours at 300°C (C). The photos are taken 5s after adding 100 μL of sodium lye, while in the inset, a higher volume was used (3x1000 μL) and the photos were taken after the tubes were completely dried; some droplets felt down without leaving any traces (see inset from picture B).

Four different types of textured tubes and one flat sample (D<sub>ext</sub> = 12 mm, stainless steel 1.4404) were coated by CSEM with OptoPEG – a very hydrophilic coating. The stainless steel tubes were cleaned with detergent (5 % of Extran MA 02 in water) prior to coating deposition. The dip coating method was used. The precursor solution was OptoPEG dissolved with 1 % PBS buffer. The tubes, after dipping in the OptoPEG solution, were incubated for 2 h at room temperature in the dark. After that, the tubes were dried first with nitrogen and then under vacuum (10<sup>-2</sup> mbar) for 1.5 h. Curing via UV irradiation was done for 2 min (350 nm, 7.6 mW/cm²). Except for sample 5, there are no visible changes on the surface of tubes No. 1, 2, 3 and 4 after functionalization. One sample (Sample 5) had small corrosion points before the coating deposition and after the treatment a pitting corrosion was observed and it was thus not included in further investigations.

Wetting experiments were performed using a micropipette and DI water to assess the influence of the hydrophilic coating. The sample code includes the short name of the coating and if it is textured or not (OPTO\_f – OptoPEG coated flat tube, OPTO\_t1 to OPTO\_t3 – OptoPEG coated tube with different texturing types). The maximum wetted width is presented in Figure 15.



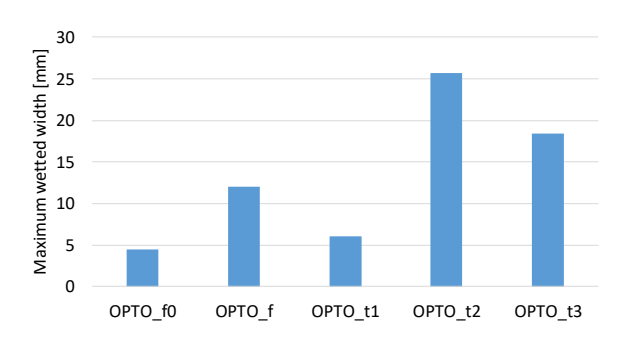


Figure 15: Wetting performance of the samples with CSEM hydrophilic coating OptoPEG.

Compared with the non-coated case (OPTO\_f0), all the samples with hydrophilic coating show a better wetting behaviour expressed as the maximum wetted width. Also, the textured samples, depending on the texture, may present a better wetting behaviour as the flat one.

# 2.3.4 Investigations regarding the stability of surfactant and concentrated sodium hydroxide solutions

The prepared surfactant solutions (0.1 to 1 wt.%) are clear and homogenous at room temperature, both for DHSS (Figure 16) and Triton™ QS-15. However, in time, precipitation and/or surfactant phase separation was observed, when the solutions are kept at room temperature for more than 1 month.



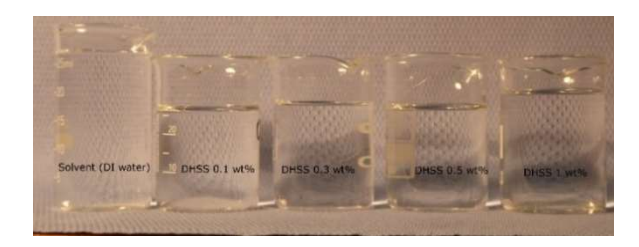




Figure 16: Surfactant (DHSS) solutions with different concentration after preparation (left) and after one week of ageing at room temperature (right) - visible modifications in case of solutions with DHSS concentration higher than 250 ppm.

The best wetting behaviour was registered for surfactant concentrations equal to 1000 ppm. A surface wetting experiment was made using the aged surfactant solution. In this case, the wetting of the testing fluid, after precipitation, was not considerably affected. However, the precipitate formation (Figure 17 and Figure 18) might have an influence on the pumping system. A similar behaviour was observed in the case of NaOH - H2O- Triton system.





Figure 17: Precipitation in case of DHSS 1000 ppm and NaOH 45 wt.% after one month of exposure at room temperature.

Figure 18: Surfactant phase separation after 48 days at room temperature in case of Triton 1000 ppm and NaOH 45 wt.%.

### 2.3.5 Increasing the residence time of the sorbent in the water vapour

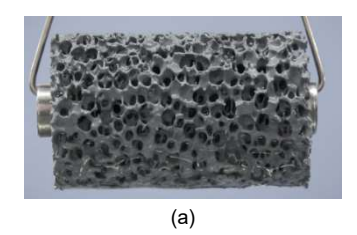
For the residence time, the use of ceramic foams and their surface wetting was analysed using aqueous sodium hydroxide and aqueous lithium bromide.

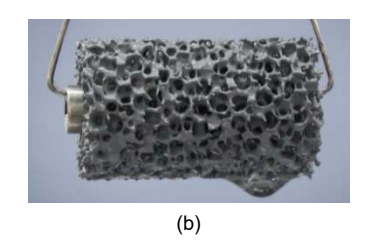
Silicon carbide is an ultra-hard covalently bonded material. It is very stable and it can react with sodium hydroxide only in the presence of oxygen and at temperatures over 350°C to produce sodium metasilicate. As in the ABSTOREX project the working temperature is below 100°C and the atmosphere is oxygen free (vacuum), SiC can be used as a cover for the stainless steel tubes (Figure 19) from the tube bundle in order to increase the residence time. Samples from Hofmann CERAMIC GmbH with porosity ranging from 10 to 30 PPI, where PPI (Pores Per Inch) represents the number of pores in one linear inch (length) were tested. To avoid contamination of sorbent solutions with CO2 from the air, experiments were performed into a glove bag.

In a first step, the wetting behaviour of the ceramic foam was investigated. Different volumes of aqueous solutions of NaOH and LiBr ranging from 100 µL to 1000 µL were used. The preliminary wetting experiments have indicated that all the tested ceramic foams have a hydrophilic behaviour, both with concentrated NaOH (45 wt.%) and with LiBr (54 wt.%) solutions.

After that, the effect of the ceramic foam on the residence time of the sorbent in the water vapour was assessed. Stainless steel tubes (Dext=10 mm, Dint=8 mm) wrapped by ceramic foam (Dext= 50 mm, Dint=10 mm) with different porosity were immersed in concentrated sodium hydroxide solutions (45 wt.%). Higher residence time is obtained for the sample with smaller pore size (30 PPI, Figure 19, a). Larger pores favour a faster flow of the concentrated sodium hydroxide solution, thus a lower residence time follows (Figure 19, b, c).







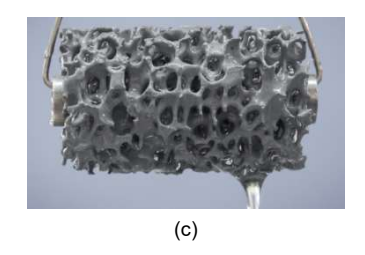


Figure 19: Hydrophilic SiC ceramic foam with pores partially filled by concentrated aqueous sodium hydroxide; the porosity is ranging from 30 PPI (a) to 20 PPI (b) and 10 PPI (c), where PPI represents the number of pores per inch.

Following a similar procedure like the one mentioned above, a mass uptake measurement campaign was performed. Silicon carbide samples with different porosities and different thermal fluids which are used as sorbent in the 1 kW prototype were investigated.

As shown in Figure 20, the smaller the pores are, the higher is the mass uptake. This means that the sorbent is "kept back" and thus the residence time of the sorbent in the sorbate vapour is increased. The foam acts like an "intermediate storage". Nonetheless, another contribution of the foam is to increase the gas-liquid interface. By high mass uptake (by small pore sizes), the foam is partially clogged with the liquid, what may reduce the contact area and therefore the mass exchange.

The concentrated sodium hydroxide solution, having the highest viscosity (see Figure 20, right), has also the higher mass uptake. An interesting observation is that the addition of surfactants reduces not only the surface tension (which leads to improved surface wetting), but also the viscosity. The viscosity of the sodium hydroxide solution with surfactant (Triton 1000 ppm) is reduced to a value between the one corresponding to water and lithium bromide solution. This is an important aspect which must be considered when setting up the technological parameters (e.g. mass flow) in the 1 kW test rig.

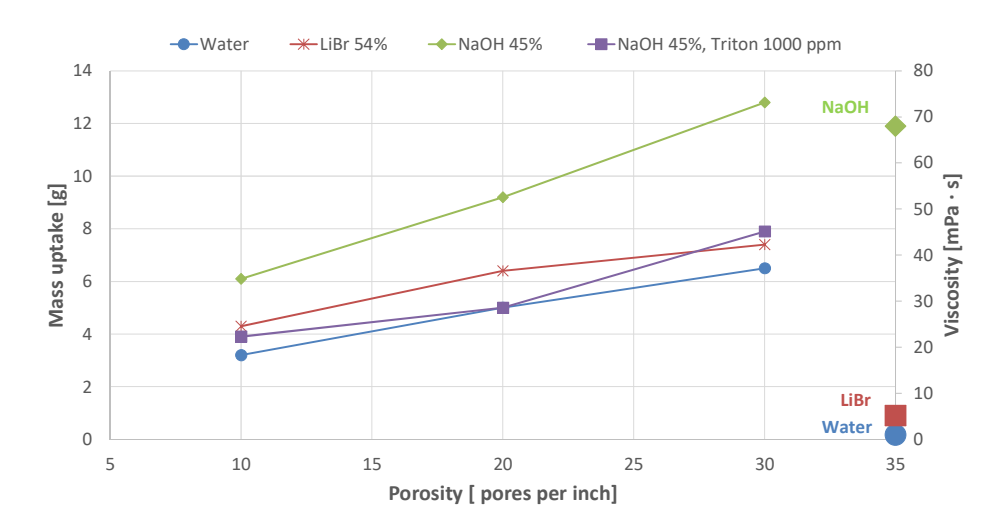


Figure 20: Mass uptake of different thermal fluids (concentrated NaOH with/out surfactant addition and concentrated LiBr) depending on the ceramic foam's porosity and viscosity of the different solutions.

As the ceramic SiC foam are intended to be used in a low pressure system for longer period of time, the durability and degassing effect is critical and it was assessed. In vacuumed containers, degassing of the ceramic foam was already known and investigated (either presence of impurities during the fabrication process and/or permeation of the air present in the cavities generated during the fabrication process). The degassing process generally stops after 1-2 days and is even accelerated by increased temperature of 90 - 100 °C.



A curing was carried out at ambient temperature on the SiC ceramic samples and followed with satisfactory results. However, an immersion in sodium hydroxide triggered a new degassing process. A constant pressure was only reached after about one month of immersion. Moreover, after this month, the mechanical stability of the foam samples proved to be severely affected (Figure 21, left). After an immersion time of 2 months, the sample proved to be totally destructed (Figure 21, right).





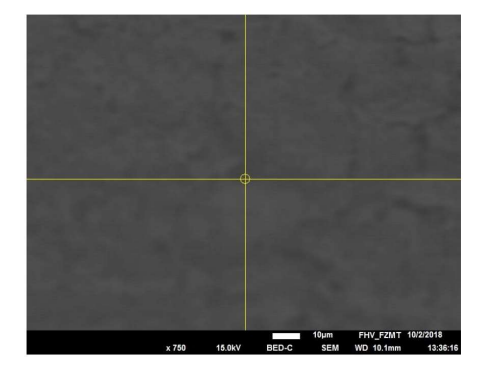
Figure 21: Left: ceramic foam after one month of lye exposure (colour change and crumbling); right: dissolved ceramic foam sample after a two-month immersion in concentrated sodium hydroxide.

In this condition, to protect the experimental facility from damages (filter clogging, blockage of the dosing pump, abrasion of the Coriolis sensors etc.) it was decided not to do any experiment with the ceramic foam in the 1 kW test rig.

To explain the degradation of SiC foams, Scanning Electron Microscopy with Energy Dispersive X-Ray Spectroscopy (SEM/EDX), one of the best known and most widely-used surface analytical techniques, was used (Prof. B. Friedel FH Vorarlberg). The results indicated that the ceramic foam (30 PPI) is contaminated and extremely oxidized. Besides silicon and carbon, the sample contains also oxygen, aluminium and iron Figure 22 and Figure 23Figure 23). These impurities can react sodium hydroxide and/or water, e.g. aluminium oxide reacts with sodium hydroxide (concentrated solution) and water to produce sodium hexahydroxoaluminate (Eq. 3):

$$Al_2O_3 + 6NaOH + 3H_2O \rightarrow 2Na_3[Al(OH)_6]$$

Eq. 3



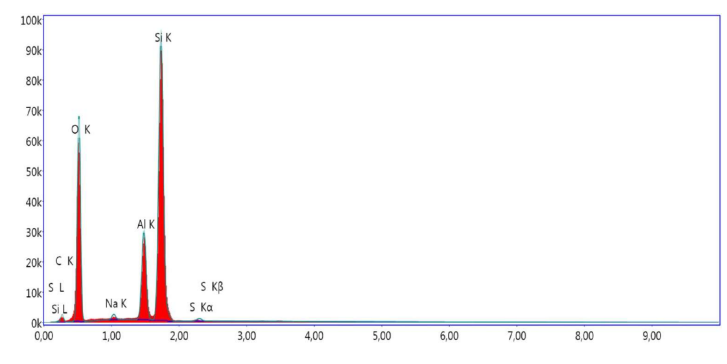
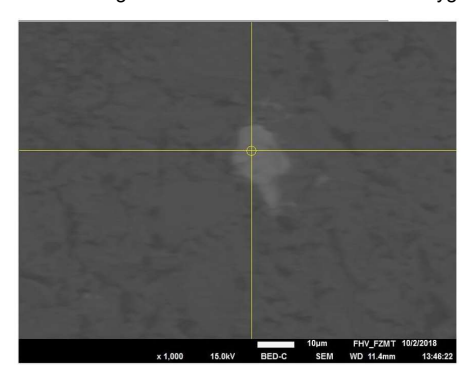




Figure 22: Scanning Electron Microscopy (SEM, left) and Energy Dispersed X-Ray emission (EDX, right) on ceramic foam (30 PPI) showing that the SiC foam contains also oxygen, besides silicon and carbon; traces of sulphur and sodium are also possible.



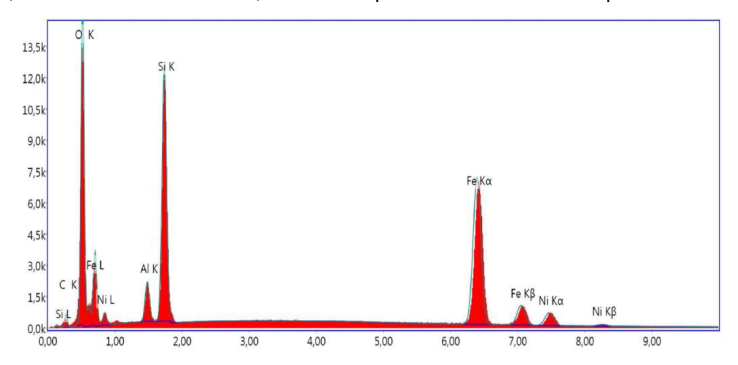


Figure 23: Scanning Electron Microscopy (SEM, left) and Energy Dispersed X-Ray emission (EDX, right) on a metal particle inclusions from the ceramic foam (30 PPI) showing that the inclusion contains also oxygen, iron and nickel.

**To summarize** the activities performed, an *improved surface wetting* of the concentrated sorbent solutions was achieved by modifying the surface chemistry: addition of surfactants in the sorbent solution, thermal annealing of the tube bundle tubes and surface roughness optimisation (mechanical texturing). The liquid sorbent *residence time* as well as the gas-liquid interface in the water vapour was increased by the use of porous SiC foams. The tested ceramic foams have a good wetting behaviour with concentrated NaOH (50 wt.%). However, because of durability issues, they were not implemented in the A-D unit from the1 kW prototype.



## 3 One kilowatt laboratory test rig

Aim of the 1 kW laboratory test rig is to assess the performances of the preselected surfactants as well as surface modifications for the heat and mass exchangers. The test rig has to be able to emulate the working condition of the power unit of a real thermochemical heat storage.

### 3.1 Experimental setup

The ABSTOREX experimental setup is shown in Figure 24. The left part of Figure 24 shows a CAD view of the absorption-desorption test rig. It comprises a power unit with the Absorber-Desorber (A-D) and Evaporator-Condenser (E-C) heat and mass exchangers. The three tanks underneath the power unit are for the sorbate (water) and for the high and the low concentration aqueous sorbent. The right part of Figure 24 shows the core 1 kW experimental setup - a detailed view of the power unit.

For the hydraulic scheme, different colours were used to differentiate between the sorbent loop (in green arrows) and the sorbate loop (in dark blue arrows). As shown on this figure, the ABSTOREX experimental setup includes the following:

- H<sub>2</sub>O loop: the components of this circuit are: a dosing pump, a heat exchanger, the water tank
  (A in the figure), the E-C and sensors (temperature, pressure and density).
- NaOH-H<sub>2</sub>O loop: has the same components as the H<sub>2</sub>O loop, a pump, the A-D and sensors. In this loop, two tanks are needed, one for the diluted lye and one for the concentrated lye. The fluid loop has different circuits according to the operation: discharging or charging mode. These circuits are driven by three three-way valves.
- H<sub>2</sub>O tank (A): has the role to store and to supply the sorbate (water) in the charging and discharging process. Thus, it is in the H2O circuit.
- two tanks for the NaOH low- (B) and high- (C) concentration solution
- A-D tank: this tank contains the A-D (absorption-desorption) heat and mass exchanger. This
  exchanger is connected either to a heat sink that emulates the heat demand in winter or to a
  heat source that emulates the solar thermal collectors in summer.
- E-C tank: this tank is similar to the A-D tank, but for water evaporation and condensation only
  and therefore connected to a low temperature heat source (in winter) or to a heat sink (in
  summer) that emulates the ground / borehole heat exchangers. The E-C tank and A-D tanks
  are connected via the vapour feedthrough a channel which allows the circulation of water
  vapours between the A-D and E-C unit in the charging and discharging processes.



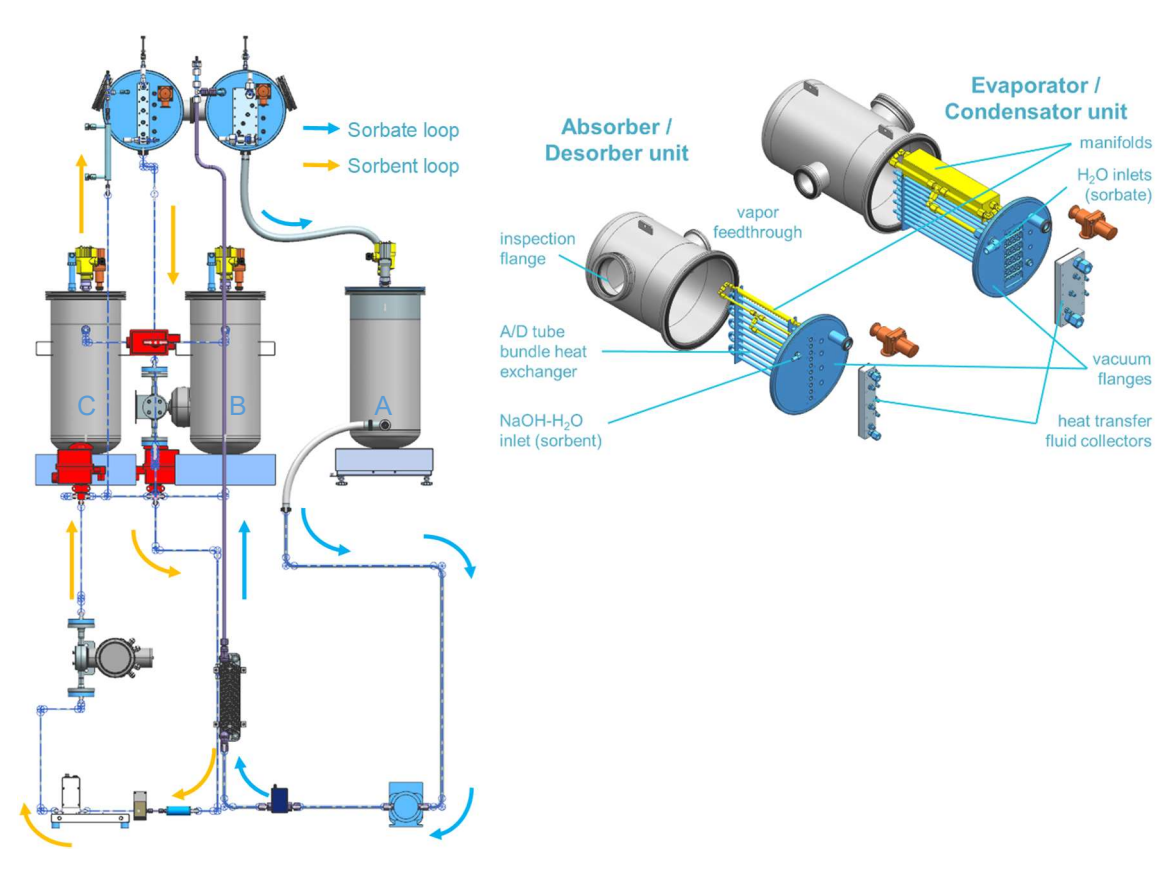


Figure 24: Front CAD view of the experimental setup (left) and detailed view of the heat and mass exchanger units (right).

Because of the seasonal separation of the processes - absorption in winter and desorption in summer – these two processes are unified in one chamber and build as one tube bundle (a compromise to reach high energy density). To analyse the absorption-desorption processes and not to limit it, the E-C unit is overdesigned.

The hydraulic scheme of the 1 kW experimental setup is given by Figure 25. In this drawing, different colours were used to differentiate between the sorbent loop (in green), the sorbate loop (in light blue) and the heat-carrying fluid loops (in purple).



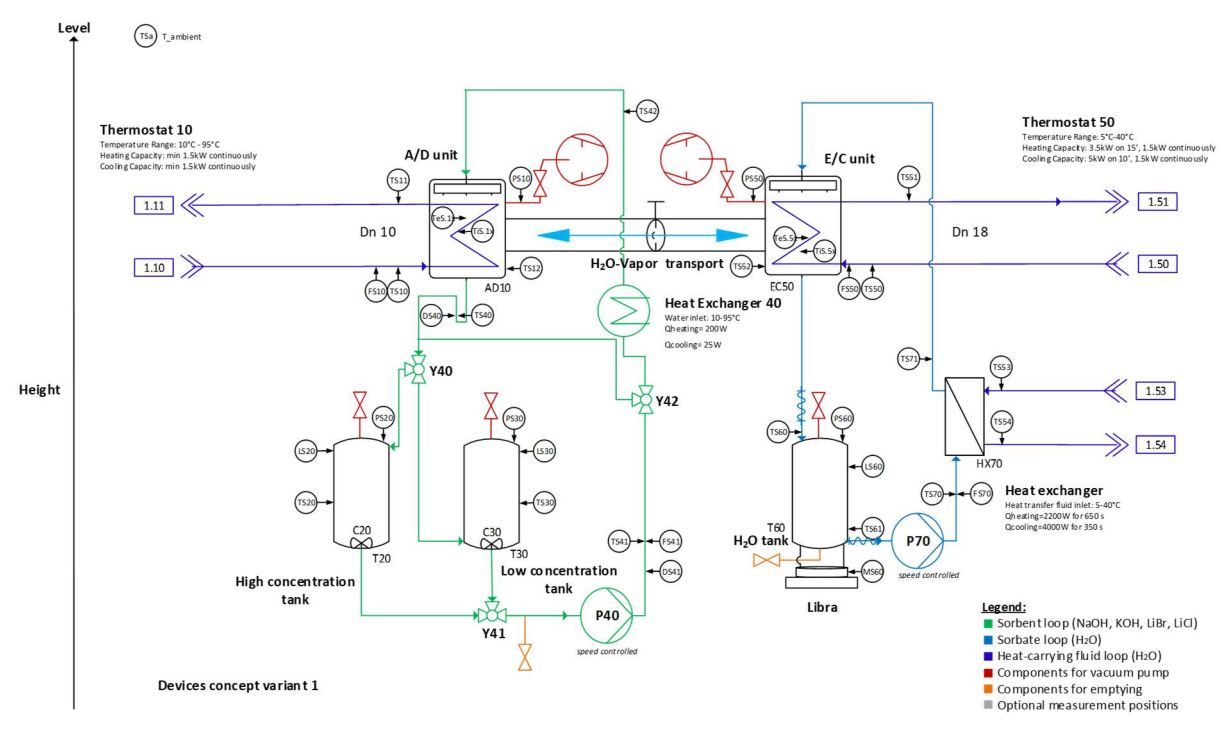


Figure 25: Hydraulic scheme of the experimental 1kW thermochemical storage experimental facility.

In addition, a nomenclature of the elements constituting the facility is given in Annex 1 and 2 of this report.

### 3.2 Heat and mass exchanger design and sizing

The heat and mass exchangers designed for the ABSTOREX system are shown in Figure 26. The manifolds are for spraying and distribution of the sorbent, the aqueous NaOH solution, in the A-D (Figure 26) and sorbate water in the E-C (see Figure 26), respectively. They enable to form a falling film around the horizontal tubes of the tube bundle heat and mass exchangers. This technology is used to increase the heat and mass transfer, and thus the performance of the reaction zone, i.e. the power unit of the setup.



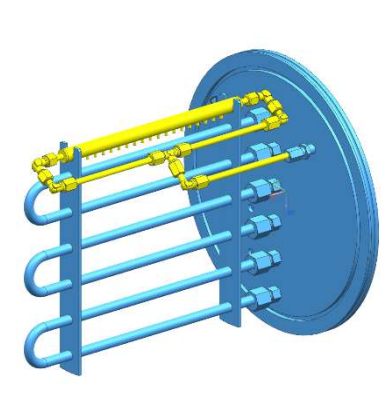




Figure 26: Isometric view of the Absorber-Desorber heat and mass exchanger with dismountable hair-pins (tube bundle and flange in blue, manifold in yellow, left) and associated picture of the built heat and mass exchanger (right).

To avoid a high consumption of auxiliary pump energy, the A-D will be used without fluid recirculation and special attention was kept to the manifold described in previous paragraph. The sorbent enters the manifold from both sides and flows through the perforated internal tube. The expected pressure losses through the perforation holes are 2.6 to 3.5 time higher (Table 1) than those due to the fluid flow through the tube, ensuring an even fluid distribution on both sides of the manifold. Table 1 also gives the pressure losses (between 15 and 17 mm liquid hydrostatic pressure) expected through the nozzles implemented in the external tube of the manifold. At least, the formation of a liquid film inside of this tube is secured, ensuring an even fluid distribution all along the manifold and thus over the tube bundle of the heat and mass exchanger.

Similar calculations and a manifold construction were made on the E-C side. But due to the possibility of recirculating water (the sorbate), the mass flow rate ranges are high enough and wetting and fluid distribution are simpler than in the A-D unit.

Table 1: Pressure losses calculation for the Absorber-Desorber manifold in both Absorber and Desorber modes and for three different concentrations.

	feeding tube (holes)			feeding tube (inside)			nozzles version 1, simu					
			2 x ø 0.001, L=0.001		1x ø 0.004, L=0.10			19	x ø = 0.0	007, L=0.006, e=0.01		
@3050Pa	m <sub>e</sub> (N+1)	wt(N+1)	ΔΡ		Ue	ΔΡ		Ue	ΔΡ		Ue	
	kg/s	kg <sub>NaOH</sub> /kg <sub>sol</sub>	Pa	mm	m/s	Pa	mm	m/s	Pa	mm	m/s	
		0	140.97	14.42	0.415	11.45	1.17	0.052	3.77E+01	3.86	0.09	
	0.00065	0.3	161.87	12.54	0.315	51.71	4.01	0.039	1.73E+02	13.44	0.07	
absorber		0.5	168.19	11.49	0.277	65.53	4.47	0.035	2.20E+02	15.03	0.06	
	0.00080	0	210.12	21.50	0.511	14.67	1.50	0.064	4.81E+01	4.92	0.11	
desorber		0.3	226.95	17.59	0.387	64.07	4.97	0.048	2.15E+02	16.64	0.08	
		0.5	231.44	15.80	0.341	81.04	5.53	0.043	2.72E+02	18.57	0.07	



For the reaction zone sizing, calculations based on a numerical model (Daguenet-Frick et al., 2015) developed in the frame of the EU COMTES project were carried out. This model was experimentally validated for the Desorber unit, but not for the Absorber unit (heat and mass exchange quite lower than predicted), whereas it appeared that the sizing of the E-C was not limiting the heat exchange. This behaviour is probably due to the water recirculation over the tube bundle. Table 2 presents the modelling results for charging and discharging processes for two extreme possible mass flow rates of the heat transfer fluid inside of the tube bundle for the final version of the four heat and mass exchangers (sorbent: NaOH-H<sub>2</sub>O).

Table 2: Modelling of the two heat and mass exchangers in charging and discharging modes (with NaOH-H<sub>2</sub>O).

		ex2-desorb	er	ex2-absor	ber	ex1-conde	nser	ex1-evaporator	
model		max	min	max	min	max	min	max	min
internal tube diameter	mm	8	8	8	8	8	8	8	8
external tube diameter	mm	10	10	10	10	10	10	10	10
horizontal tube pitch	mm	22.6	22.6	22.6	22.6	16	16	16	16
vertical tube pitch	mm	22.6	22.6	22.6	22.6	16	16	16	16
lenght of the tubes	т	0.2	0.2	0.2	0.2	0.3	0.3	0.3	0.3
number of column	-	1	1	1	1	4	4	4	4
number of row	-	10	10	10	10	10	10	10	10
m <sub>i_tot</sub>	kg/s	0.030	0.020	0.015	0.015	0.141	0.100	0.200	0.200
U <sub>i</sub>	m/s	0.62	0.41	0.30	0.30	0.71	0.50	0.99	0.99
ΔΡ	Pa	4081	1877	1166	1166	6810	3571	14352	14350
T <sub>i</sub> (1)	°C	95	95	14	14	35	35	5	5
T <sub>i</sub> (N+1)	°C	86.6	83.3	30.0	30.0	37.4	36.7	3.8	3.8
h <sub>i</sub>	W/(m2.K)	5341	3808	1850	1850	3988	3052	3399	3393
P <sub>e</sub>	Pa	7050	7050	590	590	7000	7000	710	710
rerate	-	1	1	1	1	100	50	200	150
m <sub>e</sub> (N+1)_tot	kg/s	0.00082	0.00080	0.00065	0.00065	0.0400	0.0200	0.0800	0.0600
m <sub>e</sub> (1)_tot	kg/s	0.00050	0.00050	0.00108	0.00108	0.0404	0.0204	0.0796	0.0596
Γ	kg/(m.s)	0.0016	0.0016	0.0021	0.0021	0.0167	0.0084	0.0333	0.0249
Re	-	1.22	65.00	2.33	2.33	6509.03	3269.38	0.00	0.00
wt(N+1)	kg <sub>NaOH</sub> /kg <sub>sol</sub>	0.3	0.3	0.5	0.5				
wt(1)	kg <sub>NaOH</sub> /kg <sub>sol</sub>	0.496082	0.4828	0.3	0.3				
T <sub>e</sub> (N+1)	°C	18.0	18.0	18.0	18.0	39.0	39.0	2.1	2.1
T <sub>e</sub> (1)	°C	78.3	76.3	61.7	61.7	39.0	39.0	2.1	2.1
h <sub>e</sub>	W/(m2.K)	787	786	469	469	2826	1702	5059	3934
φ <sub>i</sub>	kW	1.06	0.99	1.00	1.00	1.01	0.99	1.05	0.99



According to Table 2, a heat exchanger power of about 1 kW should be reached with a 10 tubes tube bundle on the A-D side (tube length: 200 mm). To limit the temperature difference, a tube bundle of 4 columns of 10 tubes is required for the Evaporator-Condenser side (tube length: 300 mm). Sizing of the pumps and flow meters are based on these simulations.

### 3.3 Facility building

Apart from the sensors, standard vacuum parts, as well as the tube bundles, all the components constituting the facility were in-house manufactured and pre-assembled. The setup is built with a top and a bottom part. Figure 27 shows the bottom part as well as the top part of the setup.

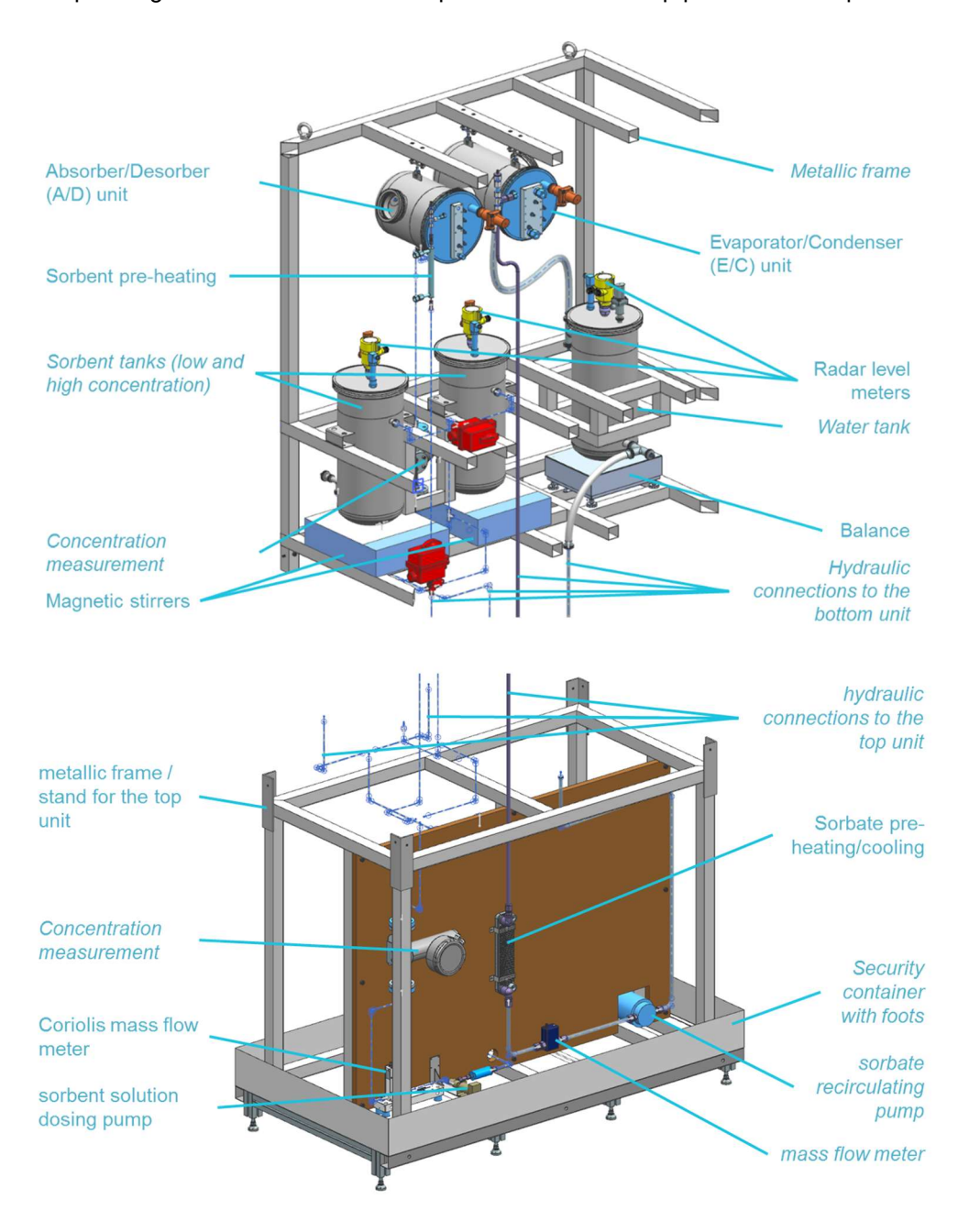




Figure 27: Isometric view of the top and bottom part of the facility with the heat and mass exchanger unit as well as the storage tanks (top) and the pumps and mass flow meters (bottom).

A passivation treatment as well as an electro-polishing were performed for all components in contact with sodium hydroxide. The result of these treatments are smooth and shiny surfaces with a higher corrosion resistance (Figure 28).

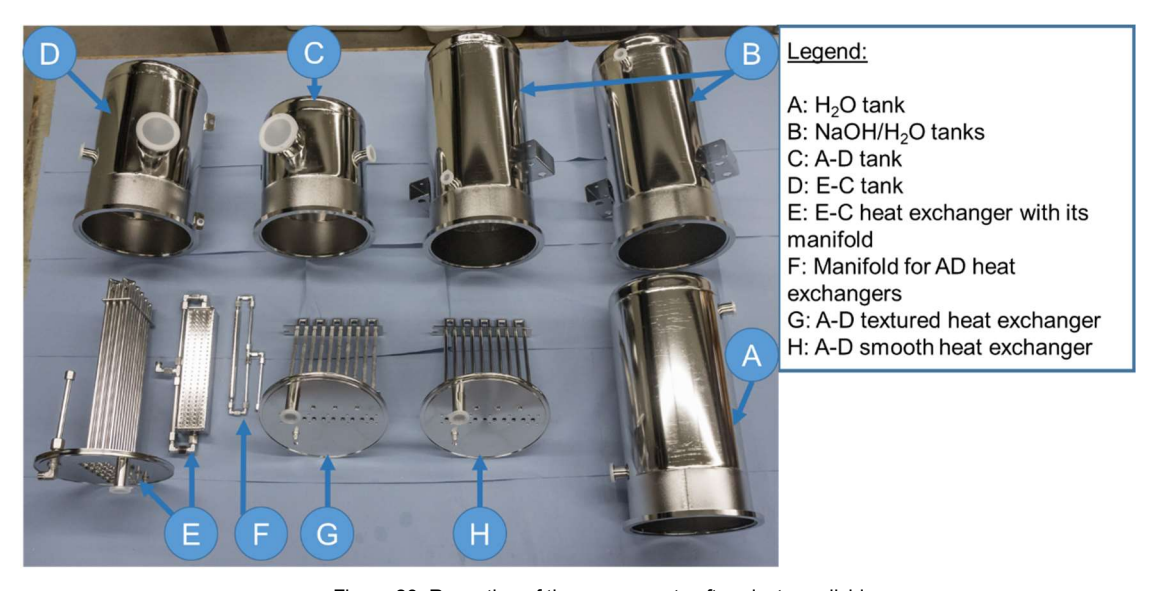


Figure 28: Reception of the components after electro-polishing.

Figure 29 shows the E-C and the A-D heat and mass exchanger units. These heat and mass exchangers constitute the "heart" of the thermochemical storage, i.e. the power unit of a storage system. They are here depicted after electro polishing, with the heat transfer fluid manifold and temperature sensors feed through installed and ready to be implemented in the setup.



Figure 29: E-C (left) and A-D (right) heat and mass exchanger in its container.

A view of the assembled facility after transportation to its final location is given by Figure 30.





Figure 30: Front view of the facility assembled at its final location/position.

### 3.4 Heat Transfer Fluid (HTF) loop

The Heat Transfer Fluid is presented in Figure 31 and it includes the heat sink and heat sources required to run the facility.

The heat sink and heat source unit consists of two water storage tanks, a 500 I cold storage (T90) and a 200 I hot storage (T80). The hot water storage will be charged up to 95 °C and the cold water storage down to 5 °C. The hot storage is charged by a power controlled electric heater (C80) of 10 kW heating capacity. With the controller, the hot storage inlet temperature (TS80) can be set to the requested water temperature. The cold storage is charged by the cooling infrastructure (compressor cooler, storage tank, etc.) of the laboratory. There, the cold source has a cooling capacity of 8 kW and the cooling loop has hydraulic separation from the experimental setup by a flat plate heat exchanger (HX90). The inlet temperature to the cold storage measured by TS90 can be adjusted by the flow rate controlled pump P90. For most of the planned experiments it will be 15 °C. This setup serves as heat source and sinks of the facility.



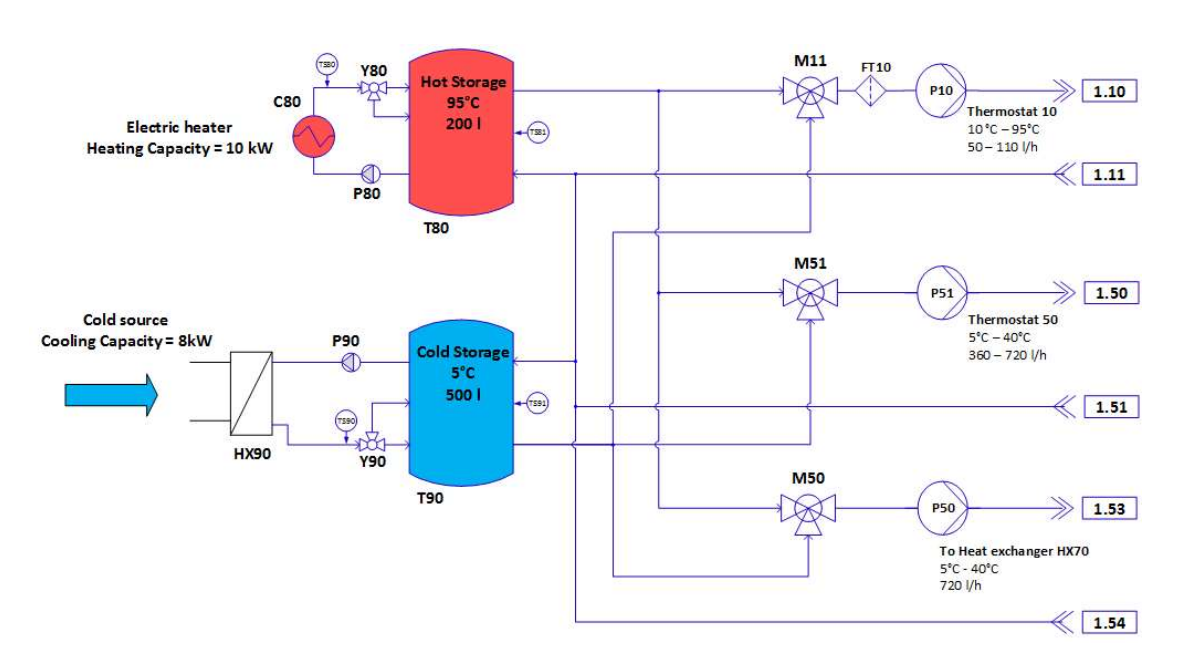


Figure 31: Hydraulic scheme of the external heat source and heat sink loops.





Figure 32: Stacked thermal storage tanks (left) with hot storage (200 l) at the top and cold storage (500 l) at the bottom to avoid fluid circulation by gravity. Right: view of the HTF distribution loops that provide the absorption storage system with thermal energy on three different temperature levels.

### 3.5 Control and DAQ

The control and data acquisition is programmed with a National Instruments CDAQ data acquisition unit. This CDAQ can be equipped (extended) with different analog and digital input and output modules. All the data will be stored on a LabVIEW programmed data base called "Citadel". Figure 33 shows the electric cabinet which comprises all the necessary electric and electronic components for the control of the experimental setup and the data acquisition.





Figure 33: View inside of the electric cabinet with the integrated measuring transducer "mPDS5" of the density sensors (top left part of the picture).

The control and data acquisition software is based on NI LabVIEW (JKI) state machine templates. The operation of the software can be done in two different modes "manual control" and "automatic control". In the manual mode, every actor (pump, valve, magnetic agitator, etc.) can be operated individually. In the "automatic mode", the system can be set in four different system states, which are: "charge", "discharge", "measure low concentration tank" and "measure high concentration tank". Figure 34 shows the LabVIEW GUIs of the absorption storage.

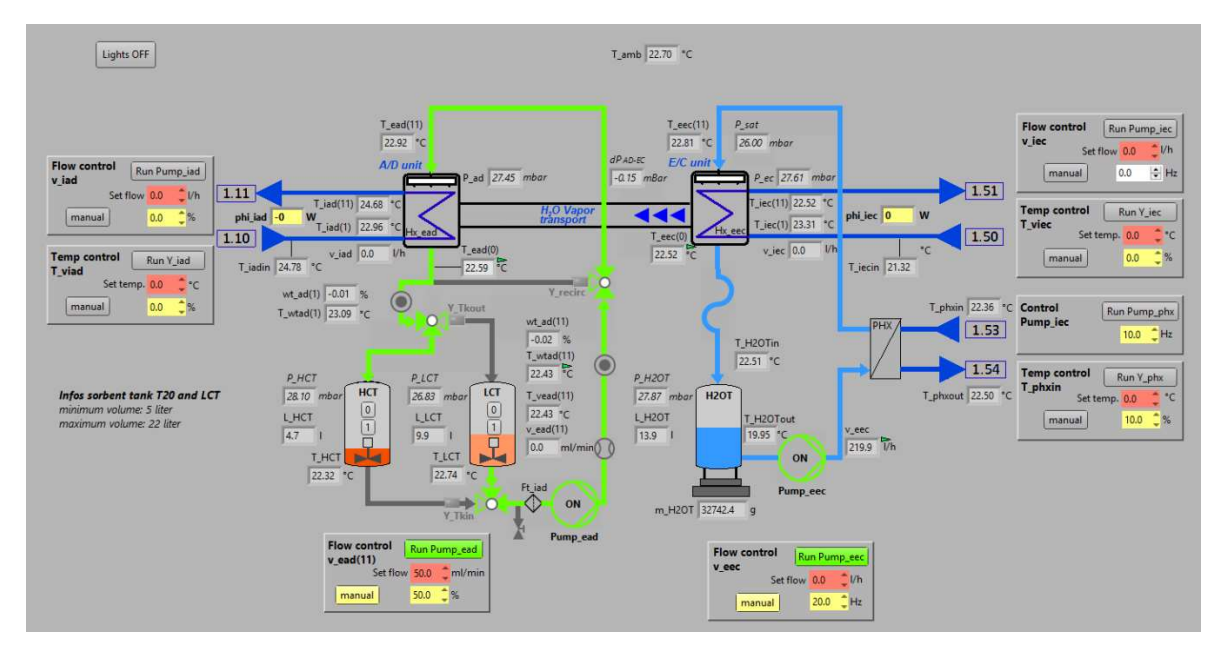


Figure 34: Improved version of the LabVIEW GUI for the experimental absorption storage setup.



## 4 Facility Commissioning

#### 4.1 Sensors selection and calibration

Using the experience gained on the operation of a former test rig{Citation}, the instrumentation concept was improved and extended on the current test rig. This later enables to evaluate the process critical parameters (exchanged power, amount of condensed/vaporised water for example) and it includes:

- 40 temperature sensors (all calibrated Pt 100 sensors) for the temperature measurement in the Heat Transfer Fluid (HTF) loops as well as on the surface of the tubes constituting the heat and mass exchangers (sorbent and sorbate temperatures);
- 5 piezo-resistive pressure transmitters (one in each chamber/tank);
- 4 flow rate measurement (2 magnetic inductive sensors, 1 Coriolis sensor and 1 oval-wheel-sensor) to measure precisely the flow rates in each of the HTF, sorbent and sorbate loop;
- 3 radar level meters (tracking of the tanks filling in real time);
- 2 density measurement sensors (precise measurement of the sorbent concentration at the inlet as well as at the outlet of the A-D unit).
- 1 precision balance (assessment of the water quantity that is vaporised / condensed).

During the design phase of the test rig, all key components were tested separately according to defined criteria (among 3 pre-selected dosing pumps, only one was retained) as shown in Figure 35.

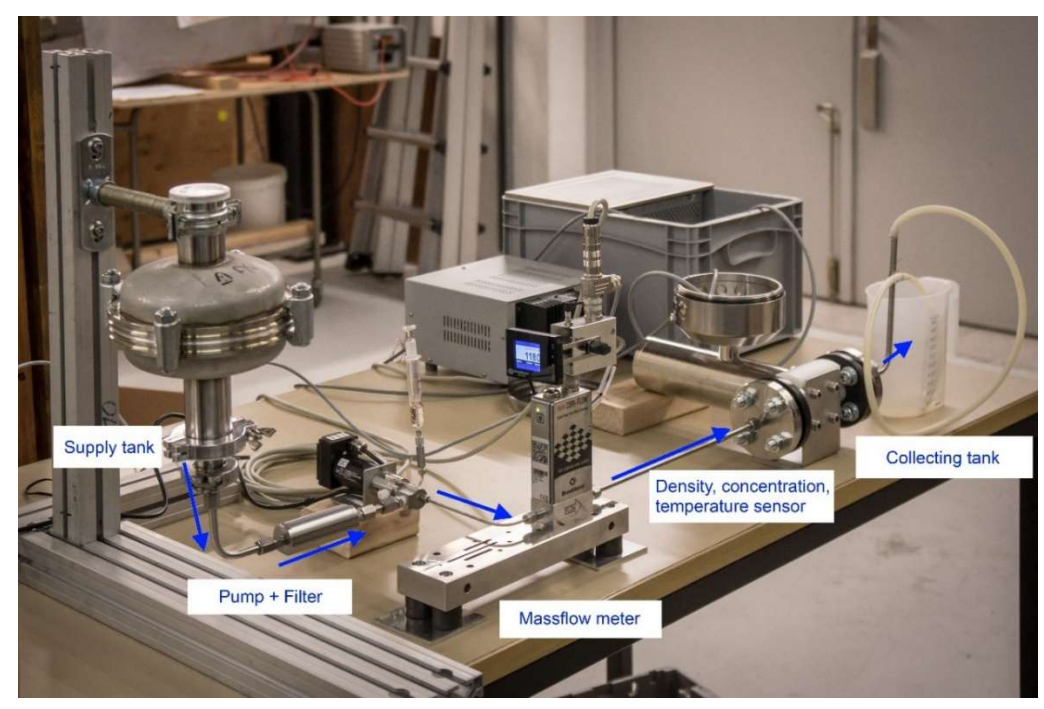


Figure 35: Setup for preliminary testing the density, NaOH concentration, temperature sensor and the mass flow meter (A-D loop).



The retained sorbent dosing pump is the HNP mzr4605. With this pump, decent vacuum leak rates were measured (about 1.5x10<sup>-6</sup> mbar·l/s) during a first measurement phase. In a second phase, cavitation issues were studied. As shown in Figure 36 (left), for a selected fluid, the cavitation pressure (minimal pressure before cavitation occurs) is a function of the mass flow rate. Figure 36 (right) gives the cavitation pressure in function of the volume flow rate set value as well as of the sorbent concentration. In the frame of the experiment, the dosing pump runs with different parameter set points. Typical operating working points are circled in red in this graph. No major cavitation issues should occur by using this pump in the test rig described paragraph 3.1.

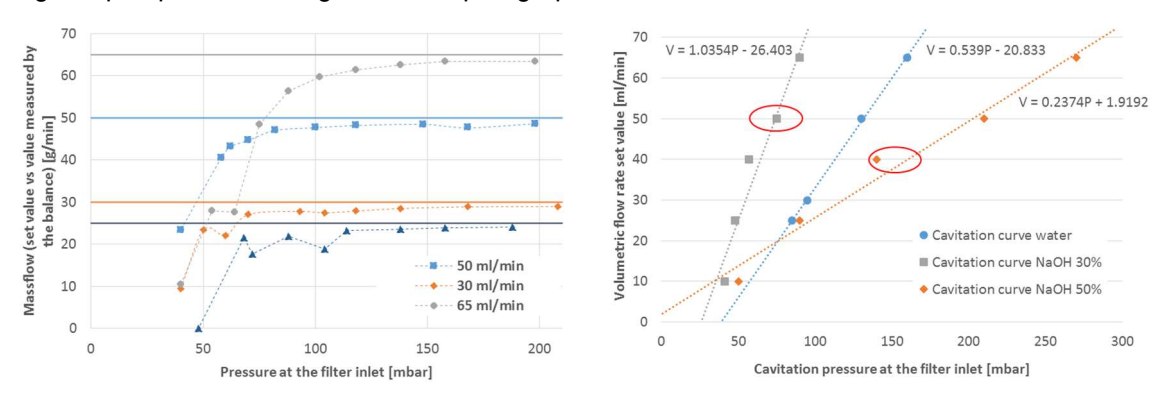


Figure 36: Comparison of the set and measured mass flow in function of the inlet pressure for water (left) and cavitation pressure in function of the set volumetric flow rate for the HNP mzr-4605 dosing pump for different sodium hydroxide concentrations (right).

After building of the test rig, a calibration procedure was followed for the pressure sensors, magnetic inductive flow sensors and temperature sensors. Scaling was carried out for the level meters and various improvement were done to improve the reliability of the sensors (introduction of ball bearings to guide the water tank, solution conductivity enhancement for the magnetic inductive flow sensor or PTFE deflector for the radar level measurement sensors, see Figure 37 right)





Figure 37: Radar level measurement sensor with water droplet (left) and with additional PTFE deflector avoiding water flowing from the cap along the sensor (right).



#### 4.2 Leak test

The closed storage is designed to operate under a low sorbate vapour pressure and the setup should be theoretically leakage free. For our experiments, a leakage rate lower than 10<sup>-4</sup> mbar\*l/s is aimed. The leakage rate can be determined by a pressure rise measurement. However, to locate a leak, two methods were used: filling the component with helium and detect the leakage with an "external" (sniffer) leakage tester, or spraying the evacuated component with helium and detect the helium with a mass spectrometer that is connected to the inside volume.

A pressure rise in function of time was performed for each component. Some parts have an acceptable leakage rate. For the others, a more detailed leakage detection with He was necessary. After several tests, all leaks were located and all components were validated (Table 3), excepted for one: the aqueous lye solution loop (NaOH-H<sub>2</sub>O). Many tests were made in this loop and all detected leaks were repaired. However, a leak in the feed pump body remained. This leak (leakage rate of 3.30\*10<sup>-4</sup> mbar\*l/s measured) is due to a pump internal sealing, which in operation is formed by the sorbent fluid film. At this status of the project it is not problematic because during the operation we expect that the sealing will function properly with sodium lye.

The assembly of the setup was performed after all components and loops (with exception of the NaOH-H<sub>2</sub>O loop) were below the acceptable leakage rate. Once the facility contains water, the minimum pressure which may be achieved is given by the vapour pressure in function of the temperature of the water. The piezoelectric sensors installed in each of the three tanks as well as in both heat and mass exchanger units are the best suitable for the considered pressure range. However, given their accuracy as well as the volume of the facility, a pressure monitoring of at least 14 days is theoretically required to quantify a leakage in the range of 10<sup>-5</sup> mbar\*l/s.

Component	H₂O loop	NaOH-H <sub>2</sub> O loop	H₂O tank	NaOH solution tank 1	NaOH solution tank 2	A-D smooth HX	A-D textured HX	E-C HX
Leakage rate (mbar*l/s)	7.63*10 <sup>-5</sup>	3.30*10-4	5.48*10 <sup>-5</sup>	7.54*10 <sup>-5</sup>	3.57*10 <sup>-5</sup>	4.88*10 <sup>-5</sup>	7.00*10 <sup>-5</sup>	7.89*10 <sup>-5</sup>

Table 3: Leakage rate of each component of the sorption test rig after corrective action.

## 4.3 Commissioning the facility

After testing and calibration of all sensors, the facility was filled with distilled water for the thermal cycling under vacuum. While keeping the functionality of the facility, working with water on the sorbent and sorbate side enables an increased security of the operator, particular in case of any defects. Thus, if something is not working properly, opening the facility and solving the problem (e.g. changing defect sensors) is much simpler compared to the system filled with sodium hydroxide solution.

During this commissioning phase, experience was gained with different sensors and actuators. Improvements or reparation were carried on:

- The magnetic stirrers: they are foreseen to avoid sedimentation/stratification in the lye tanks due to concentration differences and thus ensure to run the heat and mass exchangers in steady state conditions. However, a compromise between flat liquid surface (reliable level with the radar sensors) and good mixing had to be found. For our configuration, the optimum rotation is about 50 rpm. A major issue evidenced during the commissioning was the surface abrasion problem caused by the stirrers: in fact, the passivated protective corrosion layers are not regenerated in



the absence of oxygen. The problem was solved by ordering a commercial magnetic rod mounted on a tripod (see Figure 38). Until the rod has arrived, a glass petri dish was used as a temporary solution to protect the bottom of the tank from abrasion.





Figure 38: Scratched magnetic rods (left) and "Satellite 70" magnetic rod on a tripod (right).

- The temperature regulation of the HTF loop. First problem evidenced was the non-negligible leakage rate of one of the three-way valve (valve M11) preventing to reach high temperatures required for desorption. It was successfully replaced by two regular two-way valves as shown in Figure 39. Furthermore, to counter temperature fluctuations, especially at low mass flow rate, additional temperature sensors were implemented near to the mixing valves. Lastly, a function looking for the valve position associated with a temperature in an index was set to speed up the HTF temperature selection.
- The tightness of the vacuumed loop. A first leak was localised in the Evaporator-Condenser loop MID sensor. This leak proved not to be linked with the fittings, but with the sensor itself (composite construction, apparition of the problem after some temperature cycles probably because of thermal differential dilatation). The sensor had to be replaced by a more robust one. The second leak appeared after implementation of the repaired sodium hydroxide dosing pump. Apparently, one of the PTFE seal was not correctly positioned; a standard exchange of the sealing has solved the issue.
- The NaOH dosing pump: a reparation of this pump was carried on by the manufacturer who diagnoses a broken rotor due to a metal particle. This particle was probably stemming from the cleaning of the filter protecting the pump with tainted pressurised air.
- Density measurement sensors: after reporting the problem to the manufacturer (unclean signal especially for the concentration measurement at the outlet of the A-D unit), both (prototypes) sensors were freely replaced by an improved version.
- The last MID sensor (measuring the HTF volume flow rate on the EC side) also had to be replaced. As this loop runs under the ambient temperature, it is likely that the electronic was damaged due to condensation water.



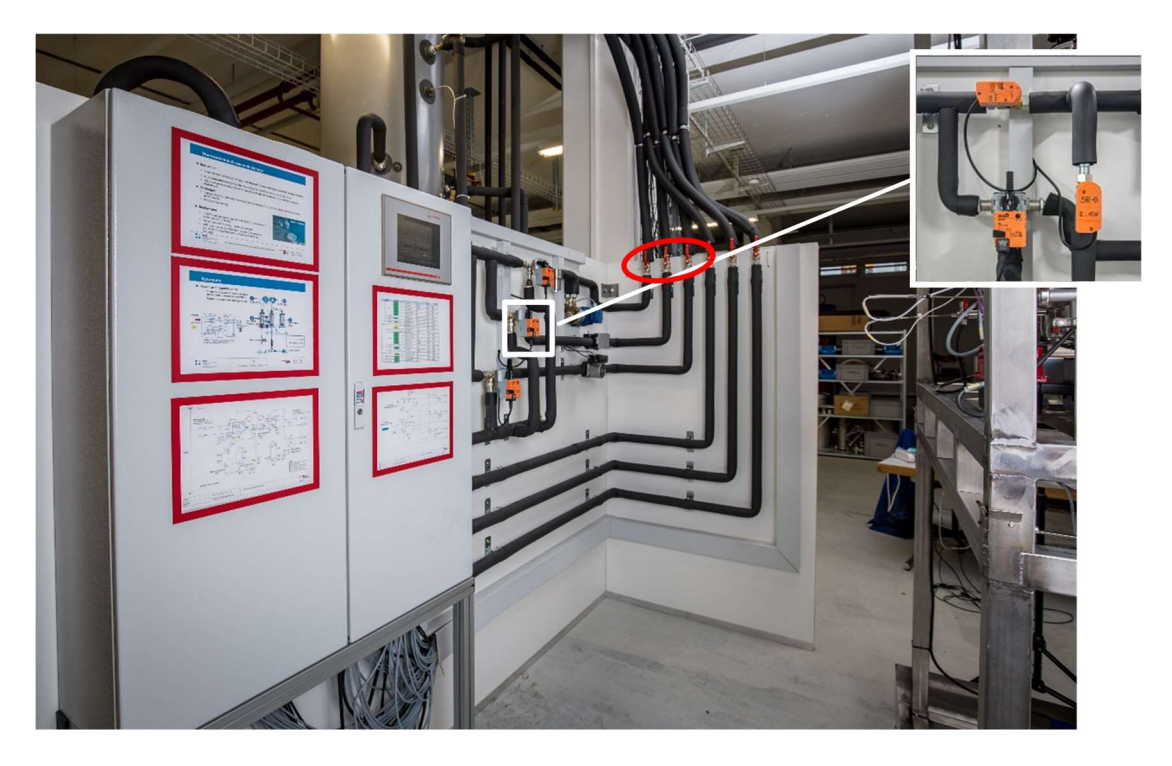


Figure 39: View of the electrical cabinet ad heat transfer fluid loops with three way valves replaced by two two-way valves (left).



## 5 Process an method

#### 5.1 Measurement and calculations

A continuous recording of the signal of all the sensors was implemented (data logging). For one process measurement point in steady state conditions, the boundary conditions were stabilised within a 15-minute (set of 900 measurement points in steady conditions, one per second). Processing of each measurement point consists in the calculation of some values (primarily heat transfer values) and time averaging the whole data set. For each value, the uncertainties (typically the "error" bars for each point) are based on statistical calculations (calculated confidence interval depending on the number of measurement for one data point). The evaluation of the data (based on the scripts and files developed for the COMTES project and adapted) follows the procedure presented in Figure 40:



Figure 40: Workflow of measurement and data processing

#### 5.2 Raw measurements

In Figure 1, typical temperature curves are shown for the heat exchanger in the A-D (HTF: triangle dots, sorbent: square dots) and E-C unit (HTF: dots, sorbate: diamonds) during an absorption experiment with the smooth tube. A constant temperature difference of 10 K was maintained between both internal HTF circuits T\_iad(1) building floor heating and T\_iec(1), the geothermal borehole source. The arrows indicate the flow direction of the respective fluids. It is nearly a cross-flow heat exchanger.

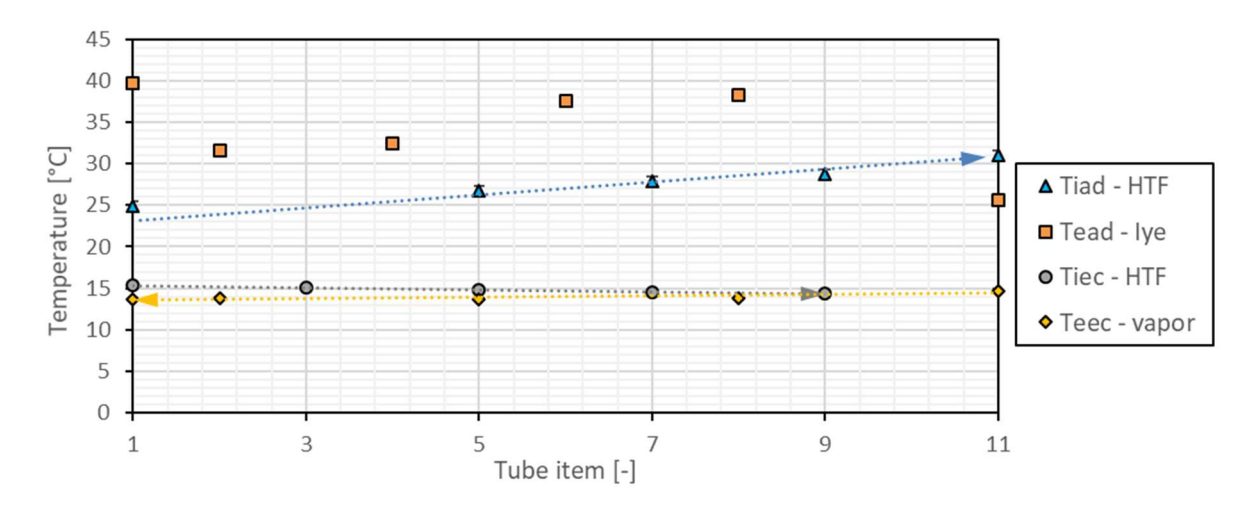


Figure 41: Temperature trend over the HX in the A-D and E-C unit.



The sodium lye temperature has a trend to increase from the inlet T\_ead(11) to the outlet T\_ead(1) due to absorption of water vapor. The released heat is transferred to the heat transfer fluid, which can be heated up from T\_iad(1) = 25°C to T\_iad(11) = 30 °C. The sodium lye is therefore cooled down from T\_ead(8) to T\_ead(2). The inlet temperature T\_ead(11) of the sodium lye corresponds to the room temperature where as T\_ead(1) is located in the sump of the container and monitors the back flowing of the diluted sodium lye solution. In the sump on the bottom of the A-D unit, a large surface area is provided and the water vapours still react with sodium lye. As a result, T\_ead(1) measures the highest temperature. Actually, no heat is exchanged with any HTF and the energy of the back flowing sodium lye is lost. It could be used in an advanced prototype to pre-heat the inlet stream v\_ead(11). During desorption, a pre-heating would also help to gain more evaporation power. Otherwise, the fluid is only heated up over the first stages of the falling film heat exchanger and evaporation occurs later on. The pre-heating would therefore help to reduce the volume of the reaction zone.

The sodium lye temperatures almost decrease linear [T\_ead(8) to T\_ead(2)], which indicates that the heat exchanger was practically uniform wetted during the measurement. The error bars are small, which shows that the path of the droplets did not change. However, for a more accurate statement, pictures should be taken from the heat exchanger during the experiment. The evaporation temperature in the EC unit is constant due to the resulting phase change of the fluid.

#### 5.3 Facility function tests

As the facility is designed to investigate the Absorber performances, one main point was to check that the E-C unit is not limiting the heat and mass exchanges. For this purpose, the influence of the recirculated volume flow rate of sorbate (liquid water) on the exchanged heat is shown on Fig. 2 for both desorption and absorption process.

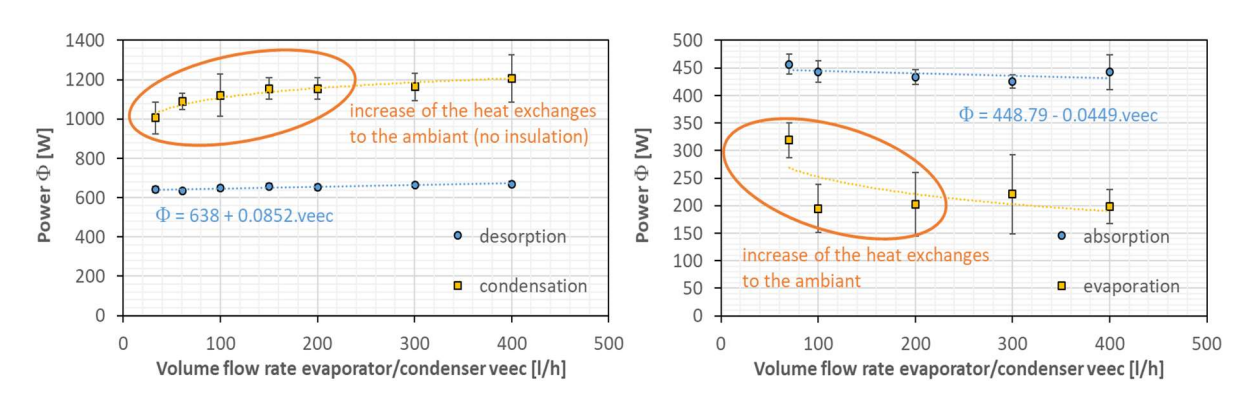


Figure 42: Evolution of the power on both A-D and E-C tube bundle in function of the sorbate volume flow rate recirculated on the E-C unit for both desorption (left graph) and absorption (right graph) processes.

According to the left graph of Figure 42, before installing the thermal insulation of the E-C unit, this recirculated volume flow rate had some influence on the heat exchanged on the Condenser side at room temperature ( $T_{room}$  of 25 °C) and condensation temperature of  $T_{E-C}$  of 15 °C. Therefore, the E-C unit was thermally insulated. The second graph from the right side of Fig. 2 shows the measurements results after insulation (same value of parameters  $T_{room}$ ,  $T_{E-C}$ ). Even if some minor influence of the volume flow rate can be observed on the Evaporator power, the power on the Absorber remains quite constant. However, despite of thermal insulation of the E-C unit as well as of the water tank and the sorbate pipes, it turned out that the E-C loop exchanges a lot of heat with the surrounding. In fact, the sorbate recirculation lead to a huge heat exchange area in comparison to the A-D loop where the heat



exchanges with surrounding are negligible. For this reason, in the following measurements performed and analysis of the results, the power measured on the A-D unit were a priority.

#### 5.4 Measurement campaigns

The following experiments were performed on the smooth and textured tube HX (with and without surfactant in the latter case).

Absorption experiments: the temperature in the condensation unit was chosen equally to a borehole source. The parameters presented in Table 4 were determined in different pre-experiments and were chosen accordingly, if not stated otherwise. The HTF volume flow in the A-D unit was chosen higher than the optimal flow for the experiment in order to overcome the slow temperature control and achieve steady state thermal conditions. An overview over all the conducted experiments can be found in attachment Annex 3. The influence of varying sodium lye volume flows as well as those of the HTF temperature difference between the A-D and E-C units (ΔT = Tiad(1) - Tiec(1)) and the volume flow of the heat transfer fluid were investigated.

Table 4: General boundary conditions for the absorption experiments.

Fixed parameters								
Variables	Units	Values	Description					
T_iec(1)	°C	15	Inlet temperature HTF E-C					
v_eec	l/h	100	Water volume flow in E-C					
v_ead(11)	ml/min	54	Lye volume flow					
v_iec	l/h	200	HTF volume flow in E-C					
v_iad	l/h	85	HTF volume flow in A-D					
wt_ad(11)	%	50	Lye start concentration					

- Desorption experiments: To compare the results of this project with results from COMTES (Daguenet-Frick et al., 2014), similar experiments were carried out. The desorption experiment was conducted only with the textured tube without surfactant. The parameters chosen are shown in Table 5. The desorption power and the concentration difference of the sodium lye were investigated for different HTF temperature difference between the A-D and E-C units (ΔT = Tiad(1) - Tiec(1)).



Table 5: Parameter table of the desorption experiments with sodium lye.

Variables	Units	Values	Description			
Varying parameters           T_iad(1)         °C         44 - 80         Inlet temperature HTF A-D           v_ead(11)         ml/min         36/ 67         Lye volume flow           ΔT         K         20 - 55         Difference between both HTF inlet temperatures           Fixed parameters           T_iec(1)         °C         25         Inlet temperature tube bundle E-C           v_eec         I/h         100         Water volume flow in E-C           v_iec         I/h         200         HTF volume flow in E-C						
T_iad(1)	°C	44 - 80	Inlet temperature HTF A-D			
v_ead(11)	ml/min	36/ 67	Lye volume flow			
ΔΤ	K	20 - 55	Difference between both HTF inlet temperatures			
Fixed parameters	s					
T_iec(1)	°C	25	Inlet temperature tube bundle E-C			
v_eec	l/h	100	Water volume flow in E-C			
v_iec	l/h	200	HTF volume flow in E-C			
v_iad	I/h	85	HTF volume flow in A-D			
wt_ad(11)	%	30	Lye start concentration			



## 6 Measurement results and discussion

#### 6.1 Absorption measurements

#### 6.1.1 Influence of the sorbent volume flow rate

The left side of Figure 43 shows the influence of varying sorbent volume flows on the absorption power. The graph on the right hand side shows the associated sodium lye concentration difference. The temperature difference between inlet temperature of the HTF at the A-D and E-C unit ( $\Delta T = T_{i\_AD\_in} - T_{i\_EC\_in}$ ) was either 10 K (triangle dots) or 20 K (square dots) and the evaporation temperature was kept constant ( $T_{i\_EC\_in} = 15$  °C). On the right graph, the concentration difference measurement shows large uncertainties. Indeed, for this measurement campaign the density sensor at the outlet of the reaction zone showed a fluctuating behaviour. It is assumed that the first version of the density sensors implemented on the test rig, based on the Coriolis principle were easily affected by external perturbation like microbubbles of vapour or non-condensed gas transported away by the sorbent.

To compare the measurement data and test the reproducibility, the first and last measurement point in a campaign of the day were conducted with a sodium lye volume flow of 54 ml/min (temperature difference of 10 K). The reproducibility is very good as the uncertainty bar covers the slight data point shift, which occurred during the measurement.

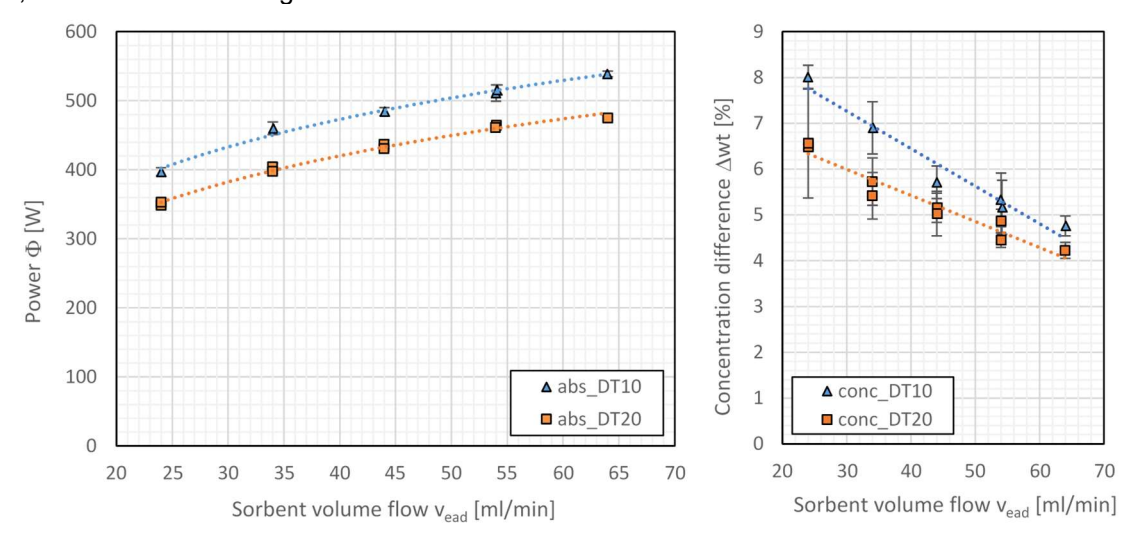


Figure 43 Absorption power (left) and concentration difference (right) in function of varying sodium lye volume flows at 10 and 20 K temperature difference between A-D and E-C unit for the smooth tube heat exchanger (HX).

The absorption power increases with increasing sodium lye volume flow. The higher flow does improve the wetting of the heat exchanger tube surfaces as well as turbulence on the tubes and as a result, the power increases according to logarithmic trend lines (doted lines in the graph). In the same time, the concentration difference decreases linearly with increasing volume flow rate, probably due to the reduction of the residence time of the sorbent in the heat and mass exchanger i.e. the sorbate vapour.

In general, the same trend is visible at both temperature difference levels. With high temperatures at the Absorber HTF inlet ( $\Delta T = 20 \text{ K}$ ), a slightly lower absorption power (about 10%) can be observed than for  $\Delta T = 10 \text{ K}$ . The achieved concentration difference is also affected by the temperature difference (the



lower the temperature difference is, the higher the concentration difference  $\Delta$ wt). However, this dependence is reduced at high sorbent flow rates; it seems that in this case the pressure differences between A-D and E-C (linked with the temperature difference itself) have less effect on the efficiency in comparison to the sorbent volume flow rate.

Practically, depending on the sorbent volume flow, different flow modes over the heat exchanger can be achieved. As the volume flow (resp. Reynolds number Re) increases, a transition from droplet to column or even sheet flow can occur (Roques and Thome, 2003). The increase of the Re number is linked to a rise of the turbulence but from a certain given Re number the wetting area can't be further increased whereas the residence time can even be reduced. However, in the considered test rig, the pump limits the volume flow rate and in these conditions, the droplet mode prevails. High sodium lye mass flow rates enable to increase the absorption power but on the other hand, this high mass flow rates are linked with a reduction of the concentration difference. As this concentration difference  $\Delta c$  is directly linked with the compactness of the thermochemical storage (the higher  $\Delta c$  the higher the stored energy), a compromise between power and concentration decrease will have to be found regardless of the heat exchanger (HX) shape.

Figure 44, left compares the power output from the absorption depending on different volume flow of the sodium lye for different heat and mass exchangers (smooth, textured, textured with addition of Triton in the solution). A temperature difference of 10 K between Absorber and Evaporator inlet temperature was chosen for this measurement campaign.

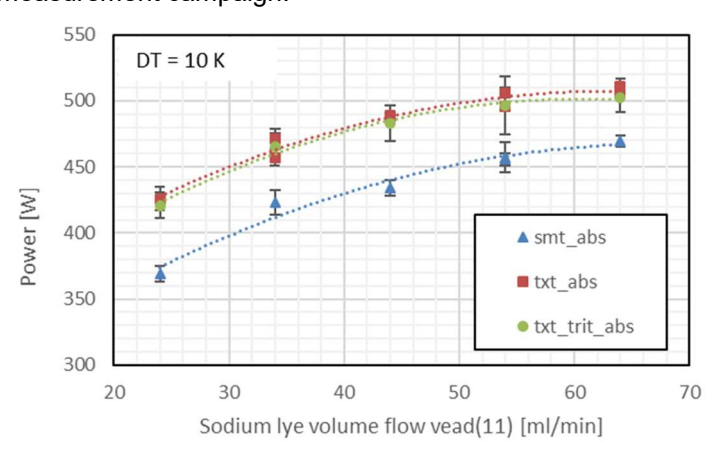


Figure 44: Power output for different sodium lye volume flow rates at DT = 10 K.

According to this figure, the use of textured tubes has a significant influence on the power output (about 20 % of improvement), whereas the addition of surfactant brings no major improvement of the output power.

#### 6.1.2 Influence of the sorbent volume flow rate (textured tubes)

On the left hand side of Figure 45, the absorption power and the HTF outlet temperature in function of the HTF volume flow rate are shown. The dotted red line indicates the transition from laminar to turbulent flow inside of the textured tubes of the A-D unit. On the right hand side, the influence of the heat transfer volume flow on the sodium lye temperature (maximum reachable temperature in adiabatic conditions) and heat transfer fluid outlet temperature are shown. The temperature of the sodium lye was averaged over the heat exchanger.



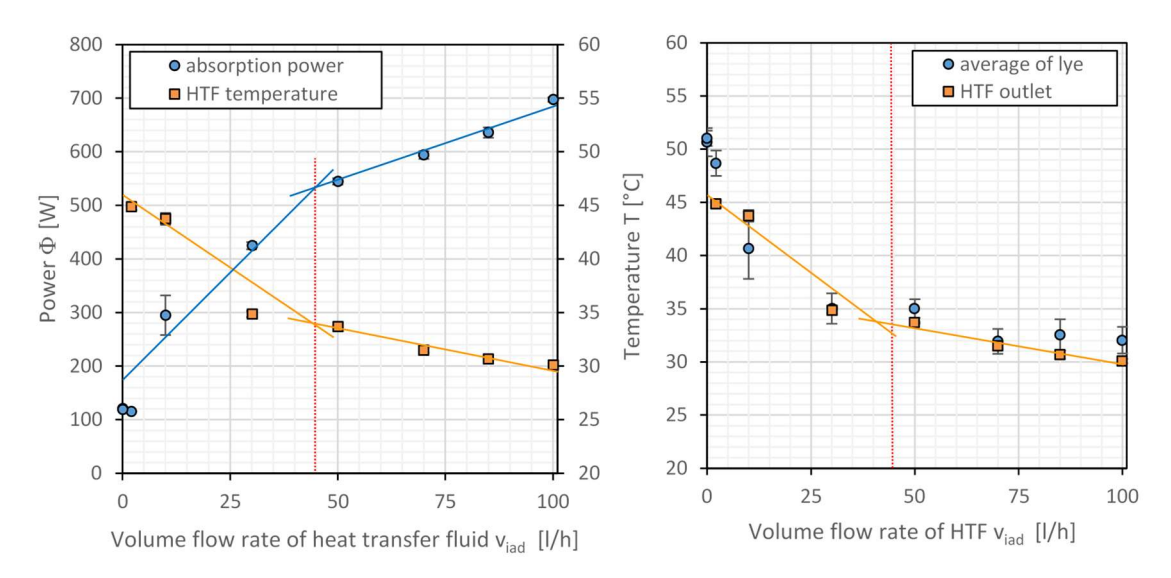


Figure 45: Comparison of the absorption power (left) and the associated temperature difference (right) as a function of the HTF volume flow rate for the textured tube heat and mass exchanger.

According to (Rotta, 1956) a transition from laminar to turbulent flow begins, when the Reynolds number exceeds 2300 inside of a tube (volume flow rate above 45 L/h, for the considered geometry). This transition explains the slope discontinuity of the linear regression observed on both graphs of Figure 45. The absorption power increases with increasing heat transfer fluid volume flow rate. On the other hand, the outlet temperature decreases as, by a constant temperature difference ( $\Delta T = Ti\_AD\_in - Ti\_EC\_in$ ), more energy can be transported out of the system by increasing fluid flow rate. For the final application, an optimal working point (compromise between output power and HTF fluid temperature) will have to be found.

At the minimal fluid flow rate, the stagnation temperature of the sorbent could be measured and is around 50 °C. In these conditions, the HTF temperature could not be measured precisely with the current test rig. In fact, the temperature sensors are placed to measure the temperature at the outlet of the tubes and not directly in the heat exchanger tube itself. However, as 50 °C is reached by the sorbent, a maximal temperature lift of 30 K between the Evaporator HTF inlet temperature and the Absorber HTF outlet temperature is practicable. With a borehole as low temperature heat source, the system may be used for building heating applications at low temperature or for pre-heating of domestic hot water.

# 6.1.3 Influence of the temperature difference between Absorber and Evaporator inlet for smooth and textured heat exchanger

In this section, measurement of both, smooth and textured version of the A-D heat exchanger are shown. The smooth (triangle dots), textured without surfactant (square dots) and textured with surfactant (disc dots) heat exchangers are compared and their absorption power is shown in Figure 46 on the left hand side. Furthermore, the concentration difference due to absorption at different temperature differences between the A-D and E-C unit is shown on the right side.

As written in section 4.3, the first version of the density sensors implemented on the test rig were affected by external perturbation like microbubbles of vapor or non-condensed gas carried away by the sorbent. However, this prototype version of the density sensors was replaced by improved ones, which turn out to be much more reliable, before the textured tube experiments were conducted. The concentration measurement error bars are consequently smaller for the textured tube experiments.



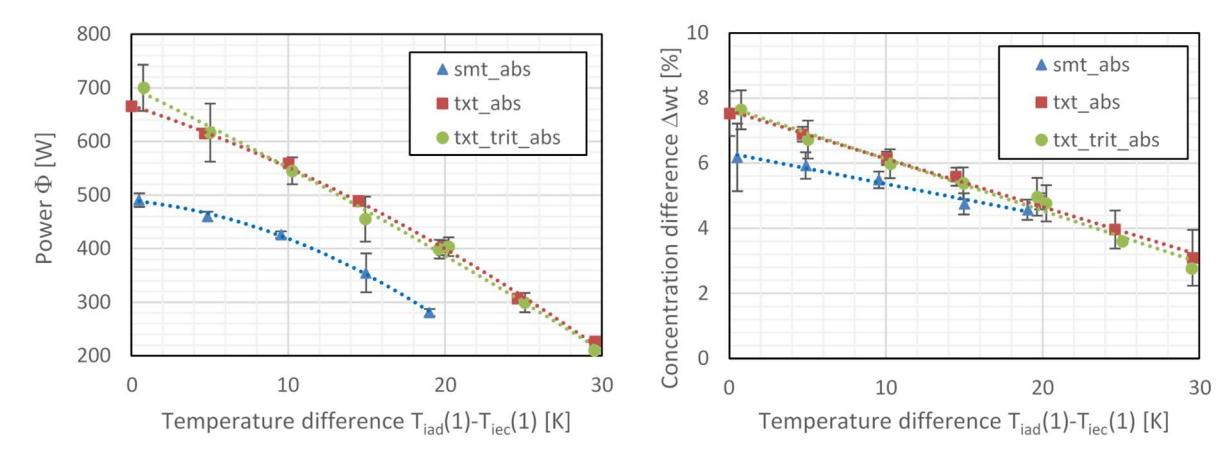


Figure 46: Comparison of the absorption power (left) and the associated concentration difference (right) as a function of the temperature difference for the smooth and textured tubes (with and without surfactant).

As expected and already explained in section 6.1.2, the absorption power decrease with increasing temperature difference. With the textured tube shape heat exchanger, an absorption power up to 20 % higher was achieved compared to the power with the smooth tube version, whereas for Triton no significant increase was noticed. The wetting has improved as it can be seen on Figure 47 for the textured tubes and for the Triton case. The droplets fall more along invisible tracks for the smooth HX, whereas for the textured HX and Triton the surface is wetted over its full visible length. Both residence time and wetting enhancement results in a higher concentration difference and therefore in a higher absorption power.

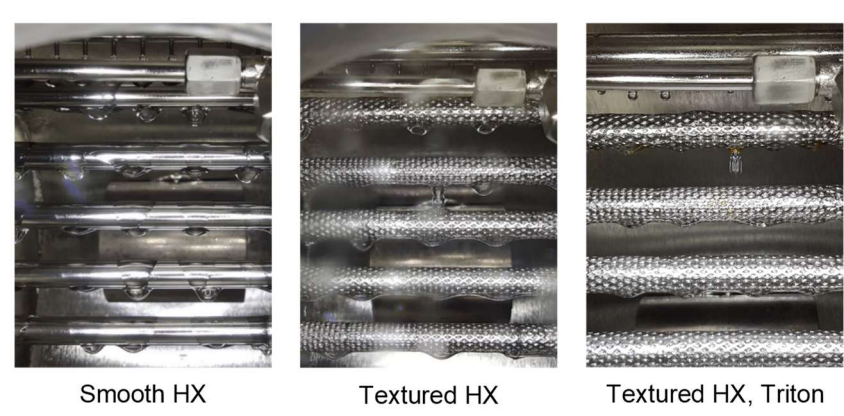


Figure 47: Evolution of the wetting on both tube bundle types in the A-D unit. Smooth tubes on the left (droplet mode) and textured without resp. with triton on the middle resp. right (transition to column mode). A higher wetting of the textured tubes at the same volume flow can be observed.

Despite of the increase of the absorption power noticed with the textured second generation of A-D heat exchanger, the aimed power of 1 kW was not reached for the absorption process. This goes also along with the concentration difference: a maximal reduction of 7.5 wt.% was achieved instead of the 20 wt.% targeted. In contrast, desorption measurements on the textured A-D showed that both expected power as well as concentration difference can be reached in this working mode and design. This shows that the insufficient results obtained in the absorption process are linked with the high viscosity of the high concentrated sodium lye solution. This viscosity itself prevents a good wetting of the tube bundle surface as well as appropriate residence time inside of the heat exchanger (exposition time of the sorbent to the sorbate vapour). Therefore, a test using the surfactant to reduce the surface tension of the sodium lye was performed. Moreover, to challenge both of these weaknesses, it is foreseen to investigate the



behaviour with a third generation heat exchangers whose tube bundle is covered by ceramic/metal foams/mesh. However, the commercial SiC foam proved to outgaze (pressure monitoring in a vacuum chamber) and not to be stable on long time period. The ceramic foam of this type of heat and mass exchanger was therefore replaced by a coiled metallic mesh (currently having being implemented in the facility) and investigations on an appropriate ceramic are currently being lead externally.

#### 6.1.4 Impact of the use of surfactant

Contrary to our expectations, no positive impact on the absorption process was noticed by adding Triton QS-15 at a concentration of about 800 ppm in the sodium hydroxide solution. This result is quite surprising because in many other experiments the absorption was improved by the aid of surfactants. For example, the steam absorption into a lithium bromide solution is better with n-octanol (Daiguji et al., 1997; Eiji and Takamoto, 1993). Although any comparable experiments with sodium hydroxide and Triton QS-15 could be found, the precedent wetting tests implicated a decreased surface tension and so an improved heat transfer.

Indeed, the addition of triton may have decreased the sorbent surface tension and increased the tube bundle wetting (see Figure 47, right) even if the textured tube bundle already seems to be well wetted. However, it seems that the sorption process itself is disrupted by the presence of Triton. Indeed, according to Figure 48, showing the pressure in the A-D unit in function of the maximal sorbent temperature, all other conditions being similar, the addition of surfactant caused a slight vapour pressure increase in the Absorber chamber. As no trace of surfactant was revealed in the E-C loop, the triton should not have been present in the vapour phase and therefore this increased pressure may not be linked with the saturation pressure of the additive.

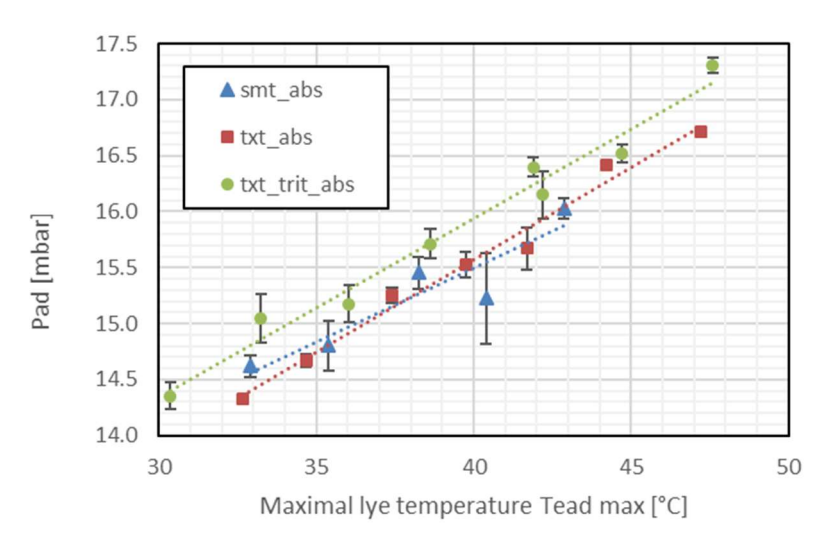


Figure 48: Pressure in the A-D chamber unit during absorption.

Another explanation of this increased pressure in the Absorber chamber may be explained by a damped absorption process. Indeed, during the storage discharging process, the Evaporator provides the required vapour at a given determined pressure (water saturation pressure). Due to the lower saturation pressure of the concentrated sodium hydroxide, a gradient of pressure prevails from the Evaporator to the Absorber chamber; at the cost of some pressure losses, the water vapour is transferred from the Evaporator to the Absorber unit. The pressure losses are linked with the cross section of the feed through (fix) as well as with the water vapour velocity: may the absorption process be damped, the mass



flow rate of water vapour (and consequently the pressure losses) will be reduced, leading to an increased pressure chamber.

From a phenomenological point of view, the surfactant, forming an additional layer at the concentred sorbent surface may hinder the water vapour uptake process. For the absorption process, sodium hydroxide is already quite delicate regarding the mass transport in comparison to other sorbent studied in the literature (high viscosity, strong concentration gradient and weak mixing of the different concentration layers), what may explain the contradictory outcomes. Further more fundamental investigations would be required to confirm or infirm this theory.

As a conclusion of the measurement campaign with surfactant, the addition of Triton QS-15 to sodium lye does not or hardly improve the absorption of sorbate vapour in a falling film Absorber using textured tubes. Regarding the associated sedimentation as well as aging issues linked with the introduction of an additional chemical specie, the addition of surfactant will not be favoured to improve the heat and mass exchanges in the near future.

#### 6.2 Desorption measurements

Like for the absorption process, the presence of surfactant does not increase significant the performances of the heat and mass exchanger for the desorption process. To investigate this point, the steam transfer depending on the power input is plotted in the Figure 49. According to this figure, a higher power is needed in the configuration with triton to evaporate the same mass of water than in the configuration without triton. Further, the maximal sodium lye temperature in the A-D unit for each measurement point is visualized on this figure. The sodium lye - triton solution seems to have higher evaporation temperature than the pure sodium hydroxide. Therefore, at same sodium lye temperature more water evaporates in the case without triton (degradation of the mass transfer).

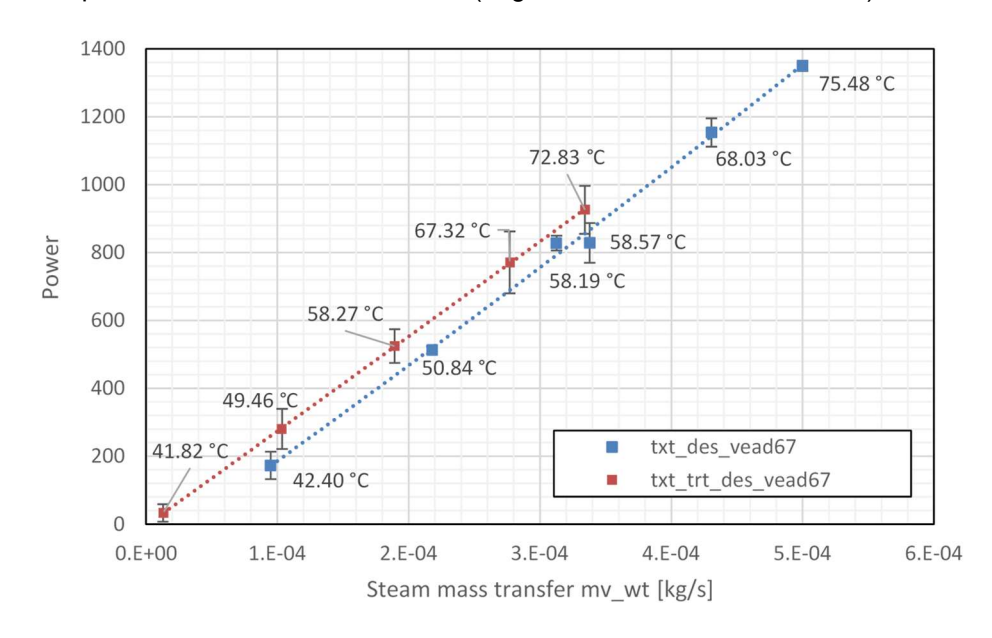


Figure 49: Evaporated steam depending on the power input during desorption; displayed temperature match to the maximal measured sodium lye temperature.

The desorption power  $\Phi$  and the absolute change in concentration  $\Delta$ wt at 36 ml/min (triangle dots) and 67 ml/min (square dots) sodium lye volume flow is shown in Figure 50. The temperature of the cooling



circuit was kept constant at 15°C and the heating circuit temperature was stepwise increased from 35 °C to 70 °C. The experiment was conducted with the textured tube only.

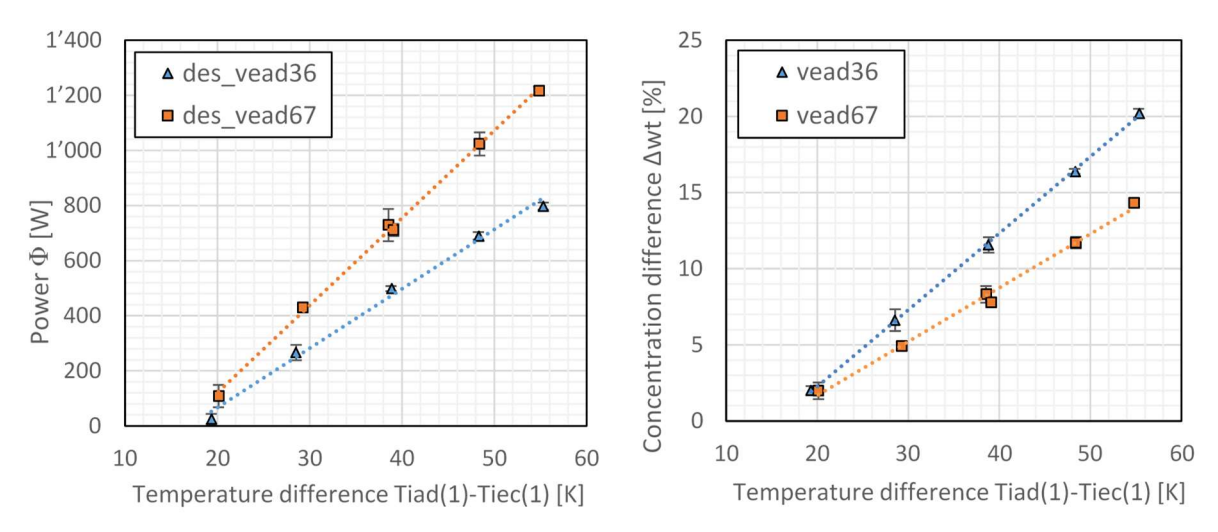


Figure 50: Influence of lye volume flow and increasing temperature difference between A-D and E-C unit on desorption power for the textured tube HX.

The power of the desorption process increases with increasing temperature difference between the A-D and E-C unit. This is the opposite behaviour than determined in the absorption experiment. The driving force for desorption is again the temperature difference between the A-D and E-C unit, which causes a pressure difference. If the lye volume flow is increased a higher desorption power can be achieved. However, at low temperature differences, the desorption power does not increase much with the flow as in this case the pressure difference seems to limit the desorption power. In return, for high temperature differences between Desorber and Evaporator, the volume flow is the bottleneck.

The reproducibility of the measurement was good as it can be seen by the two measurement points, which are overlying at 40 K for the volume flow of 67 ml/min. One measurement point was conducted as the first and the other as the last measurement point of the measurement day.

During desorption a power of more than 1 kW can be achieved depending on the available temperature difference. It was already determined in the COMTES project (Daguenet-Frick et al., 2017b), that the desorption handling is easier than absorption where the NaOH has a higher viscosity.

In comparison to the absorption experiments, a much higher concentration difference could be achieved. Depending on the volume flow, the sodium lye could be concentrated from 30 % up to 50 % as it was planned. A lower flow does increase the residence time of the lye in the heat exchanger and results in a higher concentration differences. In this case, the desorption power is however smaller because the influence of the volume flow is higher than the concentration difference.

#### 6.3 Post processing results

The heat  $(\alpha)$  and mass  $(\beta)$  transfer coefficients were determined from the absorption power measurement according to chapter 6.1. The heat transfer coefficients for the smooth (triangle dots) and textured (square dots) tubes are shown in Figure 51 in function of different sodium lye mass flow rates, when the HTF inlet temperature into the A-D unit was 25 °C and 35 °C respectively.



The linear approximation of the values are showing an extrapolation to a sorbent mass flow rate of:

$$\frac{dm_{ead}}{dt} = 2 \cdot 10^{-3} \frac{kg}{s}.$$

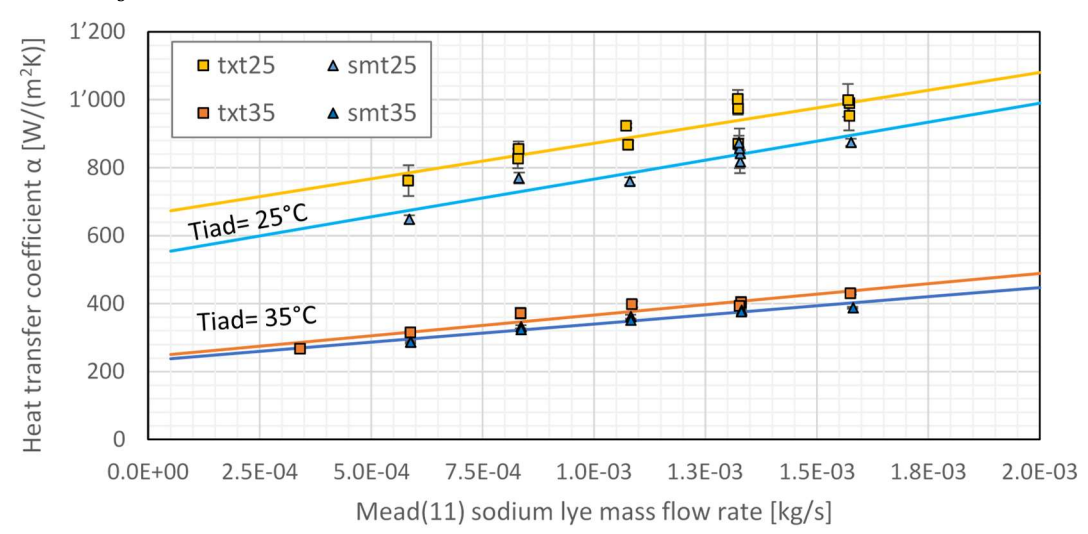


Figure 51: Comparison of the heat transfer coefficient for the textured and smooth tube HX at a HTF inlet temperature into the A-D unit of 25 °C and 35 °C at constant E-C temperature of 15°C.

The heat transfer coefficient is defined by the Nusselt number (Eq. 3), which describes the ratio between convective and conductive (sorbent) heat transfer (at boundary solid to liquid) (2013). The Nusselt Nu number itself is a function of the Reynolds number Re (which is flow dependent) and the Prandtl number Pr (which is fluid or fluid state dependent).

$$\alpha \rightarrow Nu = f(Re, Pr)$$
 Eq. 4

The same HTF mass flow rate inside of the tubes was prevailing, which leads to a constant Reynolds number (as long as the property changes of the HTF are neglected). In the experiment, the sodium lye mass flow rate (outside of the tubes) was changed, which lead to a different wetted surface of the HX, i.e. a higher sorbent flow rate caused a higher HX area wetting. The exact wetted area is (regrettably) not known due to the limited measurement equipment.

The heat transfer does increase with increasing mass flow rate but is smaller when the HTF fluid has a higher temperature. In fact, the higher mass flow rate increases the wetting of the HX. The increase of the HTF temperature does influence the fluid properties (Prandtl number) of both, the HTF inside the tubes itself and the sorbent outside the tubes. This results in the two different trend lines (Figure 51) for the heat transfer coefficient at the two temperature levels (Tiad = 25 °C and 35 °C). The effect of the fluid property change at high temperatures seems to dominate the effect of the tube shape (surface structure) since at higher HTF temperature (Tiad), only a little difference between the two different tube surface structures is visible. At lower temperatures however, a higher heat transfer is achieved with the textured tube.

Figure 52 shows the mass transfer coefficient in function of different sodium lye mass flow rates for the textured (squares) and smooth (triangles) tube HX. The inlet temperature of the HTF into the A-D unit was 25°C and 35°C. The lines show the linear extrapolation of the values to a flow rate of

$$\frac{dm_{ead}}{dt} = 2 \cdot 10^{-3} \frac{kg}{s}$$



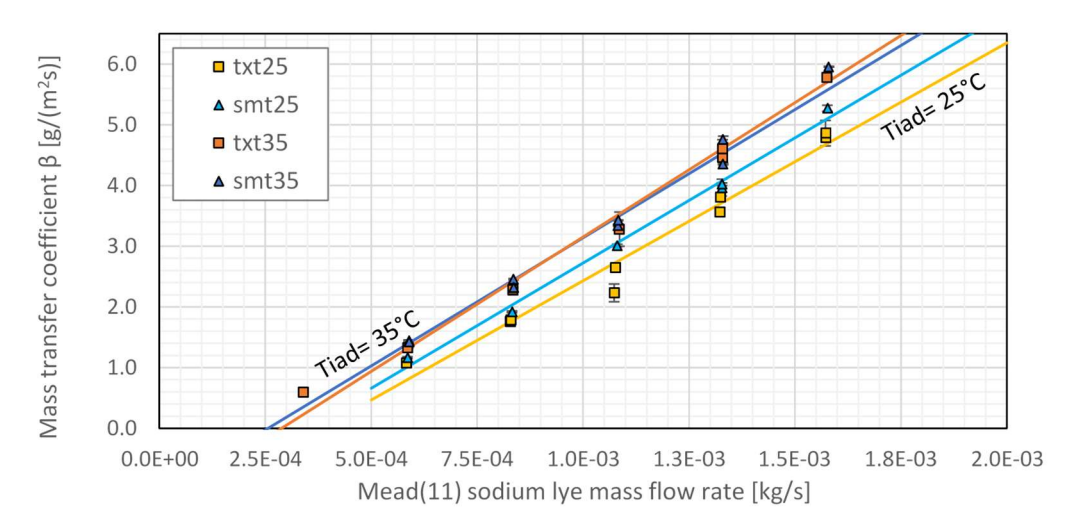


Figure 52: Comparison of the mass transfer coefficient for both heat exchanger tube surface structures in function of the sodium lye mass flow rate.

The mass transfer coefficient is dependent on the Sherwood number Sh (in analogy to the Nusselt number). It is possible to express the Sherwood number as a function of the Reynolds Re and Schmidt Sc number (Eq. 5).

$$\beta \rightarrow Sh = f(Re, Sc)$$
 Eq. 5

Again, the Reynolds number inside of the tube is almost constant due to the steady state HTF mass flow rate (as long as the property change of the HTF in the used temperature range is neglected).

The increasing sodium lye mass flow rate improves the mass transfer rate due to the increase of the wetted HX surface and turbulence. This behaviour is independent of the tube shape or the HTF temperature difference. In general, a slightly better mass transfer was achieved at higher temperatures. The tube surface structure seems to affect the mass transfer at lower HTF temperature, where the smooth tube achieves a slightly higher performance than the textured HX. The change of fluid properties at high temperatures have therefore a larger effect on the mass transfer rate than the HX structure.

Most values found in literature are for  $H_2O$  vapour absorption experiments in liquid LiBr- $H_2O$ . The conducted experiments by (Zhang et al., 2019) at higher mass flow rates and temperature of 60 °C, showed values for a smooth tube in the range of 5-10 g/( $m^2s$ ) and for a floral textured tube in the range of 15-30 g/( $m^2s$ ). Other values attained by (Beutler, 1997) with LiBr- $H_2O$  and water vapor are in the range of 35-55 g/( $m^2s$ ) at much higher mass flow rates, but at similar temperatures (35°C). Further, a heat transfer coefficient of 500-1500 W/( $m^2K$ ) was attained. With NaOH/KOH and water a mass transfer of 20-30 g/( $m^2s$ ) and a heat transfer coefficient of 350-600 W/( $m^2K$ ) could be determined.

The heat transfer determined in the experiments is in the same range as the literature values despite other working pairs were used. On the other hand, the determined mass transfer rate of the absorption experiments are at least 2 times smaller in the conducted experiments. This is attributed to the lower mass flow of sodium lye. The theoretical absorption power can be calculated with the mass transfer rate  $\beta$ , the heat exchanger surface S and the standard enthalpy change of condensation for water  $\Delta H_{v}$  with Eq. 6.



$$\varphi = S \cdot \beta \cdot \Delta H_v = 0.063 m^2 \cdot 5 \frac{g}{m^2 s} \cdot 2.5 \frac{kJ}{g} = 0.787 \ kW$$
 Eq. 6

The designed absorption power of 1 kW could almost be achieved with the textured tube HX, which was proven in the absorption experiments. The linear extrapolations to a sorbent flow rate equal to the value below was done for estimation to reach 1 kW heating power.

$$\frac{dm_{ead}}{dt} = 2 \cdot 10^{-3} \frac{kg}{s}$$

#### 6.4 System assessment

The described thermochemical storage is a closed system (only heat exchanges with the surroundings) and the process type is transported (de-coupling of the thermal energy capacity unit from the heating power unit) according to the nomenclature of (Fumey et al., 2019). In this paper, gross temperature lifts for both the (ab)sorption (GTLs) and the desorbtion process (GTLp) as well as a temperature effectiveness (TE, ratio of the sorption by the desorption temperature lift) are also defined. Such indicators are mainly linked with the sorption pair and mildly with the heat and mass exchanger technology chosen. Moreover, the considered storage proved in the absorption mode to run for a whole range of temperature conditions ( $0 < GTL_S < 30 K$ ) depending on other boundary conditions like the HTF mass flow rate: the lower the temperature lift is, the higher the output power as described in paragraph 6.1.2. The desorption process was less accurate probed (no measurement campaign investigating the sensitivity on the HTF mass flow rate) but gross temperature lifts of about 55 K may be considered in a first approximation to raise the sorbent concentration from 30 wt% to 50 wt% in one pass. Considering a realistic GTLs value of 25 K, a temperature effectiveness TE = 0.45 quite similar to those obtained by (Fumey et al., 2019) is achieved. This is not surprising as the same sorption pair is considered. These indicators constitute a good approach to determine the storage application, further investigations are currently carried on at SPF aiming to define and predict experimental storage densities (definition of indicators like the storage charging and discharging measured efficiency).



## 7 Conclusions

This report presents the main findings of the ABSTOREX project financed by the Swiss Federal Office of Energy. The project was developed at HSR University of Applied Sciences in Rapperswil by a team from the SPF Institute of Solar Technology. SPF is actively engaged to identify and develop strategic solutions to the technical challenges of the energy transition. Focusing on a compact concept for seasonal energy storage of renewables, the ABSTOREX project proposes to improve a central component of the storage, namely the Absorber-Desorber heat and mass exchanger unit.

Improvement of the heat and mass transfer by surface wetting and experiments regarding residence time of the sorbent in the water vapour are done for different stainless steel tube samples from the heat exchanger (HX). An enhanced surface wetting of the concentrated sorbent solutions was achieved by modifying the surface chemistry: addition of surfactants in the sorbent solution, thermal annealing of the HX's tube bundle and surface roughness optimisation by mechanical texturing. The potential liquid sorbent residence time may be increased by the use of porous SiC foams. Indeed, the tested ceramic foams have a good wetting behaviour with concentrated NaOH (50 wt.%). However, because of durability issues, the SiC foams were not implemented in the 1 kW prototype.

To assess the improvements from small scale surface wetting experiments, a 1kW laboratory prototype was build. This experimental test rig includes (a) the H<sub>2</sub>O loop, having as main components the E-C unit with a tube bundle HX and a water tank, and temperature, pressure and density sensors; (b) the NaOH-H<sub>2</sub>O loop with the A-D unit and same components as H<sub>2</sub>O loop, plus additional concentration sensors and two tanks for diluted and concentrated lye. Apart from sensors and standard vacuum parts, all components from the facility were in-house manufactured. A passivation treatment as well as an electropolishing was performed for all components in contact with sodium hydroxide, thus increasing the corrosion resistance. A heat exchanger power of about 1 kW was planned with a 10 tubes tube bundle on the A-D side (tube length: 200 mm) and a tube bundle of 4 columns of 10 tubes on the E-C side (tube length: 300 mm). Dedicated applications were made in LabVIEW (data acquisition), Matlab (data handling) and in Excel (for comparing the results and the effect of different parameters).

After post-processing of the measurements, the effect of different parameters was studied, e.g. the effect of volume flow rate, textured tubes or surfactant addition. The absorption power increases with increasing sodium lye volume flow and surface contact area (e.g. the case of textured tubes). The surface wetting has been improved in the case of optimized textured tubes and for the Triton surfactant when the surface is wetted over its full visible length. Both residence time and wetting enhancement resulted in a higher concentration difference and therefore in a higher absorption power. During desorption, a power of more than 1 kW was achieved depending on the temperature difference. The designed absorption power of 1 kW was almost achieved with the textured tube HX. The heat transfer determined in the experiments is in the same range as the literature values despite other working pairs were used. Compared to the COMTES system, an optimization was achieved. Further development of the ABSTOREX system include the implementation and testing of a heat and mass exchanger with a larger contact area between the sodium lye and the water vapour.

A power unit upscaling for single or multifamily house applications can be done based on the numerical model developed for the sorbent pair NaOH-H<sub>2</sub>O and water vapour. Implementation of a compact seasonal storage using the liquid sorption concept tested in ABSTOREX can be long-term solution for harvesting and store the excess of the solar energy from summer and for satisfying the need for thermal energy in wintertime.



### 8 Outlook

The next step in the further investigations will be to develop, implement and test heat and mass exchangers with a larger contact area between the sodium lye and the water vapour by using metallic meshes or foams around the tubes (Figure 53). This is expected to lead to longer residence times of the lye in the sorbate vapour as well as better performances of the system (higher absorption power with the same reactor size and higher concentration decrease, thus an improved energy storage density.

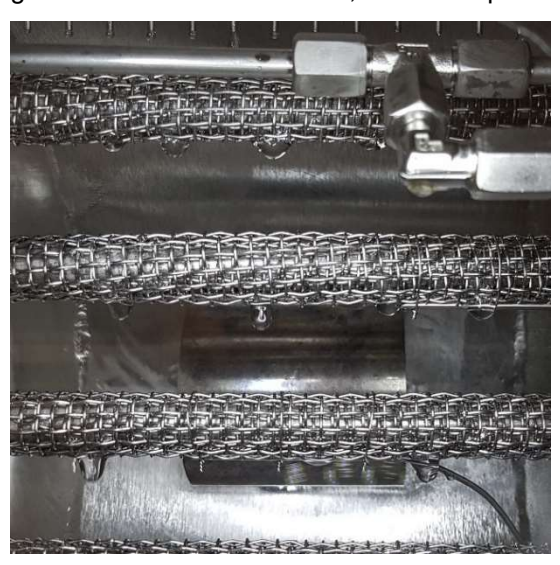


Figure 53: Implementation of a 3<sup>rd</sup> generation of heat and mass exchanger (metallic meshes coiled).

Further investigations are currently carried on at SPF aiming to define and predict experimental storage densities. Definition of Key Performance Indicators (KPIs) like the storage charging and discharging measured efficiency and methods for assessing them is planned.

## 9 National and international collaboration

Contact with the Institute of Materials and Process Engineering (IMPE) from ZHAW (Zürcher Hochschule für Angewandte Wissenschaften) was established. The aim of the work is to perform fluid contact angle measurements and to assess the suitabillity of superhydrophlic materials for the absorption unit. SPF is in discussion with the Swiss Center for Electronics and Microtechnology (CSEM) about increasing surface wetting and corrosion resistant surfaces. CSEM offered the development of a coating process with OptoPEG, which is a hydrophilic photolinker polymer developed by CSEM. Further contact to Prof. D. Poulikakos (ETHZ Department of Mechanical and Process Engineering) is established and discussions about surface treatment of heat and mass exchangers took place in Zurich. Recently, contact was taken with Prof. Ortona (SUPSI, MEMTi) in order to developp an hybrid ceramic/metal heat exchanger with specifically designed ceramic parts (additive manufacturing).



An international collaboration with the European Mission Innovation (MI) Sorption Heat Pumps is established. MI focuses on European wide collaborative technology development (http://mission-innovation.net/ ). To present our interest on this technology in the MI and our competences we contributed to the Sorption Workshop held in Pisa July 2018.

BETAL GmbH (DE) was chosen as provider to replace ETS AG. Contacts in the IEA SHC Task 58 Annex 33 working groups are established and a commitment for the lead and the coordination of the deliverable T3D3 "Description of a harmonized measurement procedure for the TCM performance under realistic application conditions" in the design of reactors is ongoing together with the task and sub-task leaders. A draft version of T3D3 was discussed at a meeting in Freiburg in June 2018. Together with Empa, the content of T3D3 and T4D1 "Basic description of investigated thermochemical storage processes and their impact on the component design" will be harmonised and discussions are ongoing.

### 10 Communication

During the whole project duration, communication was conducted by different means. In addition to the publications presented in the following paragraph, project progresses were disseminate during:

- SPF industry days (SPF Industrietag): poster presentation in March 2016, 2017, 2018, poster and slide for presentation in March 2019.
- Swiss Competence Center for Heat and Electricity Storage (SCCER HaE) annual symposiums: abstract, poster and slides for the presentation in October 2016, abstract and poster contribution in October 2017, abstract, poster and presentation in November 2018, abstract, poster and slides for the presentation in November 2016
- Presentation at the energie-cluster, HSLU Horw, March 2018
- Slides for the 6<sup>th</sup> Swiss Symposium Thermal Energy Storage, January 2019
- IEA SHC Task 58 Annex 33 working groups: presentation in Lyon, April 2017, discussions in Dübendorf, October 2017, Ljubljana, April 2018, Freiburg, June 2018, Graz, October 2018, presentation in Messina, October 2019

## 11 Publications

- X. Daguenet, F. Lichtensteiger, D. Lustenberger, P. Gantenbein, and A. Haeberle, 'Seasonal thermochemical heat storage: first measurements on a falling film tube bundle laboratory setup.', presented at the International Conference on Solar Heating and Cooling for buildings and Industry, Santiago, Chile, 2019.
- M. Dudita, X. Daguenet-Frick, L. Omlin, P. Gantenbein, and Haeberle Andreas, 'Closed sorption thermal energy storage system based on sodium hydroxide', presented at the ISEC, Graz, Austria, 2018.
- M. Dudita, X. Daguenet, L. Omlin, P. Gantenbein, and A. Häberle, 'Compact seasonal thermal energy storage for solar energy systems', presented at the EuroSun 2018, Rapperswil, Switzerland, 2018.



- X. Daguenet-Frick, M. Dudita, L. Omlin, and P. Gantenbein, 'Seasonal Thermal Energy Storage with Aqueous Sodium Hydroxide – Development and Measurements on the Heat and Mass Exchangers', presented at the 12th International Conference on the Storage of Renewable Energies (IRES2018), Düsseldorf, 2018.
- M. Dudita, X. Daguenet-Frick, and P. Gantenbein, 'Closed Sorption Seasonal Thermal Energy Storage with Aqueous Sodium Hydroxide', in Nearly Zero Energy Communities: Proceedings of the Conference for Sustainable Energy (CSE) 2017, I. Visa and A. Duta, Eds. Springer International Publishing, 2017, pp. 239–246.
- X. Daguenet-Frick, P. Gantenbein, J. Müller, B. Fumey, and R. Weber, 'Seasonal thermochemical energy storage: Comparison of the experimental results with the modelling of the falling film tube bundle heat and mass exchanger unit', Renewable Energy, vol. 110, pp. 162–173, Sep. 2017.
- P. Gantenbein et al., 'Saisonale solarthermische Absorptions-Energiespeicher mit wässrigem Natriumhydroxid als Sorptionsmittel und Wasser als Sorbat.', presented at the 12. Internationale Konferenz für Solares Heizen und Kühlen Gleisdorf SOLAR, Gleisdorf, Austria, 2016.
- M. Dudita, X. Daguenet-Frick, and P. Gantenbein, 'Seasonal thermal energy storage with aqueous sodium hydroxide experimental methods for increasing the heat and mass transfer by improving surface wetting', presented at the 11th EuroSun conference, Palma (Mallorca), 2016.



### 12 References

Akeiber, H., Nejat, P., Majid, M.Z.Abd., Wahid, M.A., Jomehzadeh, F., Zeynali Famileh, I., Calautit, J.K., Hughes, B.R., and Zaki, S.A. (2016). A review on phase change material (PCM) for sustainable passive cooling in building envelopes. Renewable and Sustainable Energy Reviews *60*, 1470–1497.

Alva, G., Lin, Y., and Fang, G. (2018). An overview of thermal energy storage systems. Energy *144*, 341–378.

Alzoubi, M.A., Akhtar, S., Fong, M., and Sasmito, A.P. (2017). Characterization of an Open-loop Seasonal Thermal Energy Storage System. Energy Procedia *142*, 3401–3406.

Aristov, Y. (2014). Concept of adsorbent optimal for adsorptive cooling/heating. (Applied Thermal Engineering), pp. 166–175.

Arteconi, A., Hewitt, N.J., and Polonara, F. (2013). Domestic demand-side management (DSM): Role of heat pumps and thermal energy storage (TES) systems. Applied Thermal Engineering *51*, 155–165.

Bacanu, G. (1991). The optimum design of heat pipe heat recovery exchanger. Transilvania University of Brasov.

Beutler, A. (1997). Stoff- und Wärmeübergang bei der Rieselfilmabsorption am horizontalen Rohr.

Brutin, D. (2015). Droplet Wetting and Evaporation: From Pure to Complex Fluids (Marseille, France: Academic Press).

Conde, M.R. (2004). Properties of aqueous solutions of lithium and calcium chlorides: formulations for use in air conditioning equipment design. International Journal of Thermal Sciences *43*, 367–382.

Daguenet-Frick, X., Gantenbein, P., Frank, E., Fumey, B., Weber, R., and Williamson, T. (2014). Seasonal thermal energy storage with aqueous sodium hydroxide - reaction zone development, manufacturing and first experimental assessments. (Aix-les-Bains, France), p.

Daguenet-Frick, X., Gantenbein, P., Frank, E., Fumey, B., and Weber, R. (2015). Development of a numerical model for the reaction zone design of an aqueous sodium hydroxide seasonal thermal energy storage. Solar Energy 121, 17–30.

Daguenet-Frick, X., Moullet, Y., Gantenbein, P., Persdorf, P., and Notter, D. (2017a). Adsorption heat pump upscaling from 1 kW to 10 kW of cooling power: experimental based modelling. In International Sorption Heat Pump Conference (ISHPC) 2017, (Tokyo, Japan), p.

Daguenet-Frick, X., Gantenbein, P., Müller, J., Fumey, B., and Weber, R. (2017b). Seasonal thermochemical energy storage: Comparison of the experimental results with the modelling of the falling film tube bundle heat and mass exchanger unit. Renewable Energy *110*, 162–173.

Daiguji, H., Hihara, E., and Saito, T. (1997). Mechanism of absorption enhancement by surfactant. International Journal of Heat and Mass Transfer 40, 1743–1752.



Delgado, M., Lázaro, A., Mazo, J., and Zalba, B. (2012). Review on phase change material emulsions and microencapsulated phase change material slurries: Materials, heat transfer studies and applications. Renewable and Sustainable Energy Reviews *16*, 253–273.

Dubinin, M.M. (1960). The Potential Theory of Adsorption of Gases and Vapors for Adsorbents with Energetically Nonuniform Surfaces. Chem. Rev. 60, 235–241.

Eiji, H., and Takamoto, S. (1993). Effect of surfactant on falling film absorption. International Journal of Refrigeration *16*, 339–346.

Florides, G.A., Kalogirou, S.A., Tassou, S.A., and Wrobel, L.C. (2003). Design and construction of a LiBr–water absorption machine. Energy Conversion and Management *44*, 2483–2508.

Fumey, B., Weber, R., and Baldini, L. (2019). Sorption based long-term thermal energy storage – Process classification and analysis of performance limitations: A review. Renewable and Sustainable Energy Reviews *111*, 57–74.

Jurado, E., Vicaria, J.M., Fernandez-Arteaga, A., Chachalis, P., and García-Martín, J.F. (2010). Wetting Power in Aqueous Mixtures of Alkylpolyglucosides and Ethoxylated Fatty Alcohols. Journal of Surfactants and Detergents *13*, 497–501.

Lee, R.J., DiGuilio, R.M., Jeter, S.M., and Teja, A.S. Properties of lithium bromide–water solutions at high temperatures and concentration. II. Density and viscocity. ASHRAE Trans.

Loewer, H. (1960). Thermodynamische und physikalische Eigenschaften der wässrigen Lithiumbromidlösung. Technische Hochschule Karlsruhe.

Löwer, H. (1960). Thermodynamische und physikalische Eigenschaften der wässrigen Lithiumbromid-Lösung. (Karlsruhe).

Löwer, H. (1961). Thermodynamische Eigenschaften und Wärmediagramme des binären Systems Lithiumbromid/Wasser. Kältetechnik *Heft 5*, 178–184.

Majmudar, S. (2014). Investigation into the effects of pH, temperature & salinity on the stability and wetting performance of sulfosuccinate surfactants.

Olsson, J., Jernqvist, Å., and Aly, G. (1997). Thermophysical properties of aqueous NaOH-H2O solutions at high concentrations. Int J Thermophys *18*, 779–793.

Pátek, J., and Klomfar, J. (2006). Solid–liquid phase equilibrium in the systems of LiBr–H2O and LiCl–H2O. Fluid Phase Equilibria *250*, 138–149.

Patterson, M.R., and Perez-Blanco, H. (1988). Numerical Fits of the Properties of Lithium-Bromide Water Solutions. ASHRAE Transactions *94*, 2059–2077.

Roques, J.-F., and Thome, J.R. (2003). Falling Film Transitions Between Droplet, Column, and Sheet Flow Modes on a Vertical Array of Horizontal 19 FPI and 40 FPI Low-Finned Tubes. Heat Transfer Engineering *24*, 40–45.

Rotta, J. (1956). Experimenteller Beitrag zur Entstehung turbulenter Strömung im Rohr. Ing. arch 24, 258–281.

Stache, H.W. (1995). Anionic Surfactants: Organic Chemistry (Marl, Germany: CRC Press).



Tracton, A.A. (2006). Coatings Materials and Surface Coatings (CRC Press).

Trigwell, S., and Selvaduray, G. (2006). Effect of surface treatment on the surface characteristics of AISI 316L stainless steel. Medical Device Materials III, Venugopalan R, Wu M (Eds): ASM International, Materials Park, OH 208–213.

Williams, M.C. (2011). Fuel Cell Seminar 2010 (The Electrochemical Society).

Xu, J., Wang, R.Z., and Li, Y. (2014). A review of available technologies for seasonal thermal energy storage. Solar Energy 103, 610–638.

Yuan, Y., and Lee, T.R. (2013). Contact Angle and Wetting Properties. In Surface Science Techniques, G. Bracco, and B. Holst, eds. (Berlin, Heidelberg: Springer), pp. 3–34.

Zhang, H., Yin, D., You, S., Zheng, W., and Wei, S. (2019). Experimental investigation of heat and mass transfer in a LiBr-H2O solution falling film absorber on horizontal tubes: Comprehensive effects of tube types and surfactants. Applied Thermal Engineering *146*, 203–211.

(2013). VDI Wärmeatlas (Düsseldorf: Springer).



## 13 Annex

## Annex 1: Laboratory test rig sensor nomenclature

Position	Measurement type	Item number	Unit	Quantity	Description	Sensor type	Manufacturer	Туре	
		TS10		1	Inlet temperature A/D unit	Pt100	Transmetra	WTMI303	
10		TS11	1	1	Outlet temperature A/D unit	Pt100	Transmetra	WTMI303	
	Temperature	TS12	°C	1	Temperature in A/D unit	Pt100 (flexible)	Transmetra	WTMI301	
		TeS.1x	1	4	Temperature on A/D exchanger	Pt100	Transmetra	WTMI303	
		TiS.1x	1	4	Temperature in A/D exchanger	Pt100	Transmetra	WTMI301	
	Pressure	PS10	mbar	1	Pressure in A/D unit	Piezoresistive pressure transmitter	Omega	PAA23-C-0.2	
	Flow rate	FS10	I/h	1	Flow rate circuit 10	Ovalradsensor	SIKA	VO06VAVHI3K	
	Temperature	TS20	°C	1	Outlet temperature tank NaOH	Pt100	Transmetra	WTMI303	
20	Pressure	PS20	mbar	1	Pressure in tank NaOH	Piezoresistive pressure transmitter	Omega	PAA23-C-0.2	
	Level	LS20	mm	1	Level in tank NaOH	Radar sensor	VEGA	VEGAPULS 64	
	Temperature	TS30	°C	1	Outlet temperature tank NaOH	Pt100	Transmetra	WTMI303	
30	Pressure	PS30	mbar	1	Pressure in tank NaOH	Piezoresistive pressure transmitter	Omega	PAA23-C-0.2	
	Level	LS30	mm	1	Level in tank NaOH	Radar sensor	VEGA	VEGAPULS 64	
		TS40		1	Outlet temperature A/D circuit NaOH	Pt100	Transmetra	WTMI303	
	Temperature	TS41	°c	1	Outlet temperature pump 40	Pt100	Transmetra	WTMI303	
	•	TS42	1	1	Inlet temperature A/D circuit NaOH	Pt100	Transmetra	WTMI303	
40	Flow rate	FS41		1	Outlet flow rate pump 40	Coriolis sensor	Bronkhorst	mini CORI-FLOW	
	Density	DS40	kg/m3	1	Outlet density A/D circuit	Density Sensor	Anton Paar		
		DS41	kg/m3	1	Outlet density A/D circuit	Density Sensor	Anton Paar		
	Temperature	TS50		1	Outlet temperature E/C unit	Pt100	Transmetra	WTMI303	
		TS51	1	1	Outlet temperature E/C unit	Pt100	Transmetra	WTMI303	
		TS52	1	1	Temperature in E/C unit	Pt100 (flexible)	Transmetra	WTMI301	
		TS53	°C	1	Inlet temperature heat exchanger	Pt100	Transmetra	WTMI303	
50		TS54	1	1	Outlet temperature heat exchanger	Pt100	Transmetra	WTMI303	
		TeS.5x	1	3	Temperature on E/C exchanger	Pt100	Transmetra	WTMI303	
		TiS.5x	1	3	Temperature in E/C exchanger	Pt100 (flexible)	Transmetra	WTMI301	
	Pressure	PS50	mbar	1	Pressure in E/C unit	Piezoresistive pressure transmitter	Omega	PAA23-C-0.2	
	Flow rate	FS50	l/h	1	Flow rate circuit 50	mid	SIKA	VMZ153S1PEG24430	
	TS60	TS60	TS60		1	Inlet temperature tank H2O	Pt100	Transmetra	WTMI303
	Temperature	TS61	°C	1	Outlet temperature tank H2O	Pt100	Transmetra	WTMI303	
60	Pressure	PS60	mbar	1	Pressure in tank H2O	Piezoresistive pressure transmitter	Omega	PAA23-C-0.2	
	Level	LS60	mm	1	Level in tank H2O	Radar sensor	VEGA	VEGAPULS 64	
	Mass	MS60	%	1	Mass in tank H2O	Weighing scale	Mettler Toledo	PBK989-AB60	
	Ŧ	TS70	°c	1	Outlet temperature heat exchanger	Pt100	Transmetra	WTMI303	
70	Temperature	TS71	1 'C	1	Outlet temperature heat exchanger	Pt100	Transmetra	WTMI303	
	Flow rate	FS70	l/h	1	Flow rate circuit 70	mid	SIKA	VMZ082S1PEG24320	
		TS80		1	Inlet temperature Hot Storage	Pt100	Transmetra	WTMI303	
80	Temperature	TS81	°c	1	Temperature Hot Storage	Pt100	Transmetra	WTMI303	
	·	TS90		1	Inlet temperature Cold Storage	Pt100	Transmetra	WTMI303	
90	Temperature	TS91	°c	1	Temperature Cold Storage	Pt100	Transmetra	WTMI303	
a	Temperature TSa		°C	1	Ambient temperature	Pt100	Transmetra	WTMI303	



## Annex 2: Laboratory test rig active elements and components nomenclature

Position	Actor type	Item number	Unit	Quantity	Description	Manufacturer	Туре	
	Pump	P10	l/h	1	Rotary valve pump	Sato AG	TMOT 051E	
10	Filter	FT10	-	1	Inline filter, 25um	HNP Mikrosysteme	F-MI3-T	
10	Mixing Valve	M11	angle	1	Ball valve with electric rotary actuator	Belimo	R506K+LR24A-SR/Z	
	AD unit	AD10	1	1	Absorber / Desorber unit	Bental	-	
20	Component	C20	-	1	Magnetic agitator IKA N		Midi MR 1digital	
20	Storage	T20	-	1	25 liter tank	self made	-	
30	Component	C30	-	1	Magnetic agitator	IKA	Midi MR 1digital	
30	Storage	T30	-	1	25 liter tank	self made	-	
	Pump	P40	l/h	1	Micro tooth ring pump	HNP Mikrosysteme	mzr-4605	
	Heat exchanger	HX40	1	1	Plate heat exchanger	unknown	-	
40		Y40	1	1	three-way ball valve	swagelok	SS-43GXS8MM-ERG10XI	
	Valve	Y41	1	1	three-way ball valve	swagelok	SS-43GXS8MM-ERG10XI	
		Y42	-	1	three-way ball valve	swagelok	SS-43GXS8MM-ERG10XI	
	Pump	P50	l/h	1	Circulation pump	Wilo	Wilo Stratos Para 15/1-11.5	
	rump	P51	l/h	1	Circulation pump	Grundfos	Grundfos UMP2 15/75	
50	Mixing Valve	M50	angle	1	Ball valve with electric rotary actuator	Belimo	R512+LR24A-SR/Z	
	Wilking valve	M51	angle	1	Ball valve with electric rotary actuator	Belimo	R512+LR24A-SR/Z	
	EC unit	EC50	1	1	Evaporator / Condenser unit Bental		-	
60	Storage	T60	1	1	25 liter tank	self made	-	
70	Pump	P70	l/h	1	Magnetic drive gear pump	IWAKI	MDG-R15 P AV IEC	
70	Heat exchanger	HX70	-	1	Plate heat exchanger	SWEP	BX8THx008/1P-SC-S 4x3/4"&16	
	Pump	P80	l/h	1	Rotary valve pump	Sato AG	TMOT 051E	
80	Component	C80	-	1	electric heater 10kW	unknown	-	
80	Valve	Y80	-	1	three-way ball valve	Belimo	R520+LR24A/Z	
	Storage	T80	-	1	200 liter hot storage	Nibe	TPSK200	
	Pump	P90	l/h	1	Circulation pump	Wilo	Wilo Stratos Para 15/1-11.5	
90	Valve	Y90	-	1	three-way ball valve	Belimo	R520+LR24A/Z	
90	Storage	T90	-	1	500 liter cold storage	Nibe	TPSK500	
	Heat exchanger	HX70	-	1	Plate heat exchanger	unknown	-	



Annex 3: Overview of conducted experiments and comparison with COMTES project

COMTES			Absorber-De	sorber					Evaporator-Co	ndenser		
			T <sub>iad</sub> (1)	V <sub>iad</sub>	wt <sub>ead</sub> (11)	wt <sub>ead</sub> (1)	v <sub>ead</sub> (11)	phi_iad	T <sub>iec</sub> (1)	V <sub>iec</sub>	V <sub>eec</sub>	phi_iec
		comment	[°C]	[l/h]	[%]	[%]	[ml/min]	[W]	[°C]	[l/h]	[l/h]	[W]
		46.6, 51.6,										
듔	absorption		55.6, 59.6,									
smooth	l gio		62.6, 67.6,									
S	aps	COMTES based	79.6						22.6		27.00	
		simulation based	14	54	50	30	25.6	1000	5	720		999-100
ے	desorption		46.6, 51.6, 55.6, 59.6,									
smooth	ior g		62.6, 67.6,									
ST	des	COMTES based	79.6	120.00	29.08		66.67		22.6	80.36	2.89	
		simulation based	95	72-108	30	48-49.6	36.1-37	999-1006	35	360-507	216-218	999-100
Abstorex			Absorber-De	sorber					Evaporator-Co	ndenser		
		0	T <sub>iad</sub> (1)	V <sub>iad</sub>	wt <sub>ead</sub> (11)	wt <sub>ead</sub> (1)	V <sub>ead</sub> (11)	phi iad	T <sub>iec</sub> (1)	V <sub>iec</sub>	V <sub>eec</sub>	phi_iec
type of HX	process	file name	[°C]	[l/h]	1%1	1%1	[ml/min]		l°C1	[l/h]	[l/h]	
					1			<u>.</u>			70, <b>100</b> ,	<u> </u>
	_	smt abs infl veec infl v4	15		48.1-48.5	38-40	45	528-573	15	200	200, 300,	195-22
oth	absorption			(50)-85-						200		
smooth	Sor	smt abs infl Tiad good v0	15, 20, 25, 30		(39)-49			383-567	15		100	131-28
Ø	s ap	smt_abs_infl_vead_DT10_v2	25	85	49.5	41.5-45		397-539	15	200	100	216-30
		smt abs infl vead DT20 v0	35	85	49.5	43-45.5	24, 34, 44, 54, 64	348-475	15	200	100	165-26
		SIIIL ADS IIIII VEAU D120 VO	30	00	49.3	40-40.0	34, 04	340-473	13	200	100	100-20
			15, 20, 25,									
	_	txt abs infl Tiad good v2	35, 40, 45	85	49.2-49.5	41-46	54	722-352	15	200	100	373-2
8	je je						24, 34, 44,					
lextured	absorption	txt abs infl vead DT10 v0	25	85	49-49.5	40-43		458-591	15	200	90	265-33
ē	aps						14, 24, 34,					
		txt abs infl vead DT20 v1 txt abs infl viad DT10 V0	35 25			<u> </u>		320-532			100 100	7-10
		txt abs inii viad D110 Vu	44, 54, 64, 63		50	40-45 30.58-	04	121-636	15	200	100	14-24
<u>re</u>	ptio	txt des infl DT vead 67 v2	74, 80		30		67	108-1217	25	200	100	273-125
textured	desorption	ot doo iiii b i voda oi ve	44, 54, 64,			31.66-	0.	100 1211		200	100	210 120
#	g e	txt des infl DT vead 36 v0	74, 80	85	30	49.77	36	25-798	25	200	100	232-95
Ę			15, 20, 25,									
ji.	<u> </u>	txt trit abs infl Tiad v1	35, 40, 45	85	49.5-50.0	42-47		767-283	15	200	100	362-1
+	absorption						14, 24, 34,					
be J	SOI	txt trit abs infl vead DT10 v0	25	85	50-49.5	41-43	44, 54, 64 14, 24, 34,	445-631	15	200	100	57-35
textured + Triton	유	txt abs infl vead DT20 v1	35	85	49.5-49.6	40-45		320-532	15	200	100	7-10
<del>e</del>		txt abs infl viad DT10 V0	25					121-636			100	14-24
+	L C		44, 54, 64,	0 00,100		10 40	0-1	.2. 500	10		. 50	
ed	ptic	txt trt des infl DT vead 67 v1	74, 80	85	30	29-38	67	33-818	25	200	100	178-96
lextured	desorption		44, 54, 64,			30.84-						
de de	txt_trt_des_infl_DT_vead_36_v0	74, 80	85	30	44.00	36	27-694	25	200	100	199-75	